Earth and Planetary Science Letters 406 (2014) 198–212

Contents lists available at ScienceDirect

Earth and Planetary Science Letters

www.elsevier.com/locate/epsl

Climate variability and ice-sheet dynamics during the last three glaciations

Stephen P. Obrochta [a,*], Thomas J. Crowley [b,1], James E.T. Channell [c], David A. Hodell [d], Paul A. Baker [e], Arisa Seki [a], Yusuke Yokoyama [a]

[a] Atmosphere and Ocean Research Institute, University of Tokyo, 277-8564, Japan
[b] Braeheads Institute, Scotland EH40 3DH, UK
[c] Department of Geological Sciences, University of Florida, 32611, USA
[d] Department of Earth Sciences, University of Cambridge, CB2 3EQ, UK
[e] Division of Earth and Ocean Sciences, Duke University, 27708, USA

ARTICLE INFO

Article history:
Received 30 November 2013
Received in revised form 24 August 2014
Accepted 3 September 2014
Available online 6 October 2014
Editor: J. Lynch-Stieglitz

Keywords:
insolation
IRD
Heinrich Event
MIS 6
MIS 8
AMOC

ABSTRACT

A composite North Atlantic record from DSDP Site 609 and IODP Site U1308 spans the past 300,000 years and shows that variability within the penultimate glaciation differed substantially from that of the surrounding two glaciations. Hematite-stained grains exhibit similar repetitive down-core variations within the Marine Isotope Stage (MIS) 8 and 4–2 intervals, but little cyclic variability within the MIS 6 section. There is also no petrologic evidence, in terms of detrital carbonate-rich (Heinrich) layers, for surging of the Laurentide Ice Sheet through the Hudson Strait during MIS 6. Rather, very high background concentration of iceberg-rafted debris (IRD) indicates near continuous glacial meltwater input that likely increased thermohaline disruption sensitivity to relatively weak forcing events, such as expanded sea ice over deepwater formation sites. Altered (sub)tropical precipitation patterns and Antarctic warming during high orbital precession and low 65°N summer insolation appear related to high abundance of Icelandic glass shards and southward sea ice expansion. Differing European and North American ice sheet configurations, perhaps aided by larger variations in eccentricity leading to cooler summers, may have contributed to the relative stability of the Laurentide Ice Sheet in the Hudson Strait region during MIS 6.

1. Introduction

Climate was relatively unstable during the last glaciation, Marine Isotope Stages (MIS) 4–2 (e.g., Dansgaard et al., 1993). Global variation and inter-hemispheric coupling were linked to reorganizations in North Atlantic thermohaline circulation that are in turn related primarily to ice sheet instability on multiple scales. Hydrographic changes resulting from freshwater forcing during Hudson Strait (HS) Heinrich Events (Heinrich, 1988; Bond et al., 1992; Hemming, 2004) decreased North Atlantic Deepwater (NADW) production, reducing northward heat flow and warming the Southern Hemisphere (Crowley, 1992). Similarly, instability and freshwater forcing on millennial scales appear to play a role in Dansgaard–Oeschger (D–O) variability (e.g., Menviel et al., 2014).

Pioneering sedimentological studies, such as those conducted at classic DSDP Site 609 from the central sub-polar North Atlantic Ocean (Bond et al., 1992, 1993; Bond and Lotti, 1995), provided the first evidence that the high-amplitude, rapid climate shifts first observed for the last glaciation in Greenland ice cores probably affected a much wider area. This work substantially advanced our understanding of Northern Hemisphere ice sheet instability and the origin of rapid climate change, as well as stimulated a vast field of interdisciplinary research. However, most observations on this important subject are limited to this most recent glaciation, mainly due to the shallow depths below seafloor of last-glacial sedimentary sequences and hence their accessibility. Much remains to be learned regarding its nature and forcing by further understanding the longer-term behavior of ice-sheet ocean interactions under differing boundary conditions during multiple glacial "realizations".

The few records of iceberg-rafted debris (IRD) variability from earlier ice ages tend to indicate significant differences between the last and penultimate glaciation (MIS 6). For example, a 500-ky IRD record from the Feni Drift (ODP 980) in the eastern North Atlantic

* Corresponding author.
E-mail address: obrochta@aori.u-tokyo.ac.jp (S.P. Obrochta).
[1] Deceased.

http://dx.doi.org/10.1016/j.epsl.2014.09.004

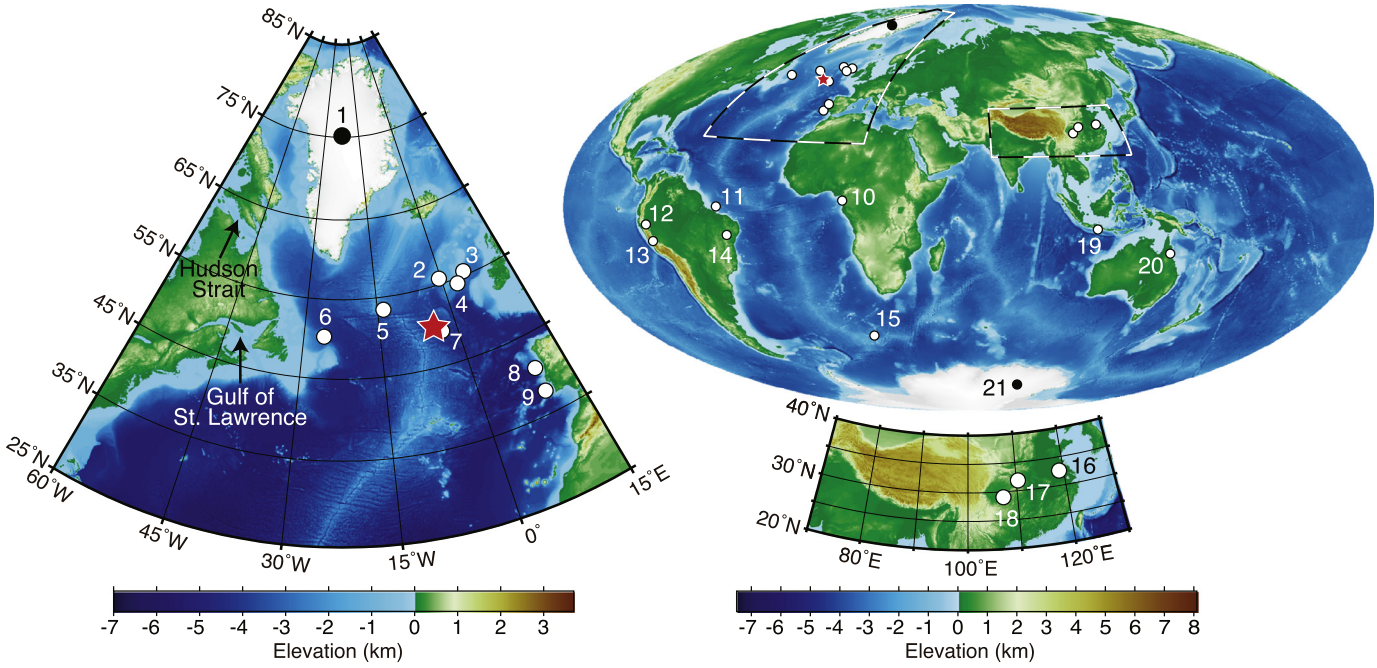

Fig. 1. Site U1308/609 (49°53′N, 24°14′W; Expedition 303 Scientists, 2006) is represented by a red star. Other sites discussed in the text are: 1) the North GRIP ice core (75°6′N, 42°20′W; Andersen et al., 2004), 2) M23414 (55°32′N, 20°17′W; Didié and Bauch, 2000), 3) ODP Site 980 (55°29′N, 14°42′W; Oppo et al., 2006), 4) V23-81 (54°15′N, 16°50′W; Bond et al., 1992), 5) Site U1304 (53°3′N, 33°32′W; Expedition 303 Scientists, 2006), 6), Sites U1302 and U1303 (50°10′N, 45°34′W; Expedition 303 Scientists, 2006), 7) V28-82 (49°27′N, 22°16′W; Bond et al., 1992), 8) MD95-2040 (40°35′N, 9°52′W; de Abreu et al., 2003), 9) MD01-2443 (37°53′N, 10°11′W) and MD01-2444 (37°34′N, 10°09′W) (Martrat et al., 2007), 10) MD03-2707 (2°30′N, 9°24′W; Weldeab et al., 2007), 11) CDH-86 (0°20′N, 44°13′W; Nace et al., 2014), 12) El Condor Cave (5°56′S, 77°18′W) and Cueva del Diamante (5°44′S, 77°30′W) (Cheng et al., 2013), 13) Pacupahuain Cave (11°14′S, 75°24′W; Kanner et al., 2012), 14) Bahia state (10°10′S, 40°50′W; Wang et al., 2004), 15) TN057-14PC (51°59′S, 4°31′E; Anderson et al., 2009), 16) Hulu Cave (32°30′N, 119°10′E; Wang et al., 2001), 17) Sanbao Cave (31°40′N, 110°26′E; Wang et al., 2008) and Linzhu Cave (31°31′N, 110°19′E; Cheng et al., 2009), 18) Yangkou Cave (29°2′N, 107°11′E; Li et al., 2014), 19) GeoB 10053-7 (8°41′S, 112°52′E; Mohtadi et al., 2011), 20) Lynch's Crater (17°22′S, 145°42′E; Muller et al., 2008), and 21) the Epica Dome C ice core (75°06′S, 123°21′E; Jouzel et al., 2007).

(McManus et al., 1999) indicates that IRD variability during MIS 6 was the least among the past five glaciations (Crowley and Hyde, 2008). Farther south, Iberian Margin core MD95-2040 also shows similar results (de Abreu et al., 2003), and recent proxies for HS Heinrich Events suggest no surging of the Laurentide Ice Sheet (LIS) (Hodell and Curtis, 2008; Hodell et al., 2008; Ji et al., 2009; Stein et al., 2009; Naafs et al., 2011; Channell et al., 2012; Channell and Hodell, 2013; Naafs et al., 2013). However, other records, such as that of core M23124 from the Rockall Plateau (Didié and Bauch, 2000), exhibit relatively increased IRD concentration during MIS 6, raising the possibility of altered circulation patterns.

To further explore the potential effects of differing boundary conditions during previous glaciations, we report a detailed, high-resolution lithic record from IODP Site U1308 (Fig. 1), a reoccupation of Site 609, that includes the previous two glaciations, MIS 6 and 8. To allow direct comparison to the MIS 4–2 petrologic tracer records from this same location (Bond et al., 1999) (Fig. 2), we employ similar methods (Bond et al., 1997) and determine the abundance of hematite-stained quartz and feldspar grains (HSG) primarily originating from the Gulf of St. Lawrence; dolomite-rich detrital carbonate (DC) sourced from the Hudson Strait; and non-weathered volcanic glass derived from Iceland (IG). These data supplement bulk lithic content data and allow us to infer lithic grain provenance and delivery mechanism (i.e., calved icebergs versus sea ice). Additional petrologic information from earlier ice ages will allow us to assess the validity of Heinrich-like layer proxies beyond the last glaciation. A detailed record from MIS 6 in particular will highlight other detrital constituents to which these proxies may be sensitive, while also potentially identifying important drivers of climate change in the apparent absence of major LIS surging. Given the lack of an ice-core record prior to MIS 5 on Greenland, the nature of HSG variability in marine cores during glacial intervals beyond the last one is important to determine whether similar conditions existed.

2. Background

2.1. Study area

Sites 609 and U1308 were occupied 20 years apart at the same location on the upper-middle eastern flank of the Mid-Atlantic Ridge, approximately 250 km south of the Charlie Gibbs Fracture Zone, between the modern North Atlantic subpolar and subtropical gyres (49°53′N, 24°14′W, 3871 mbsl; Fig. 1). During the last glaciation, the Polar Front was displaced southward of its modern location, creating steep SST gradients in this area (e.g., CLIMAP Project Members, 1976) and resulting in a concentrated zone of iceberg melting and IRD deposition, i.e., the "IRD Belt" of Ruddiman (1977). Site 609 recorded pronounced surface hydrographic changes that were interpreted to reflect stadial–interstadial swings in the position of the Polar Front (Bond et al., 1993). Thus, Sites 609/U1308 are strategically positioned to record changing climate conditions in the North Atlantic Basin and surrounding continental regions. The rationale for drilling Site U1308 was to recover a demonstrably complete stratigraphic section using modern coring methods to replace the remaining material from the Site 609 cores that is now in poor condition (Expedition 303 Scientists, 2006).

2.2. Last glacial variability at Site 609

Results from classic DSDP Site 609 (Fig. 2) were particularly important to the development of the current paradigm view of millennial climate variability. This site preserved a record of DC

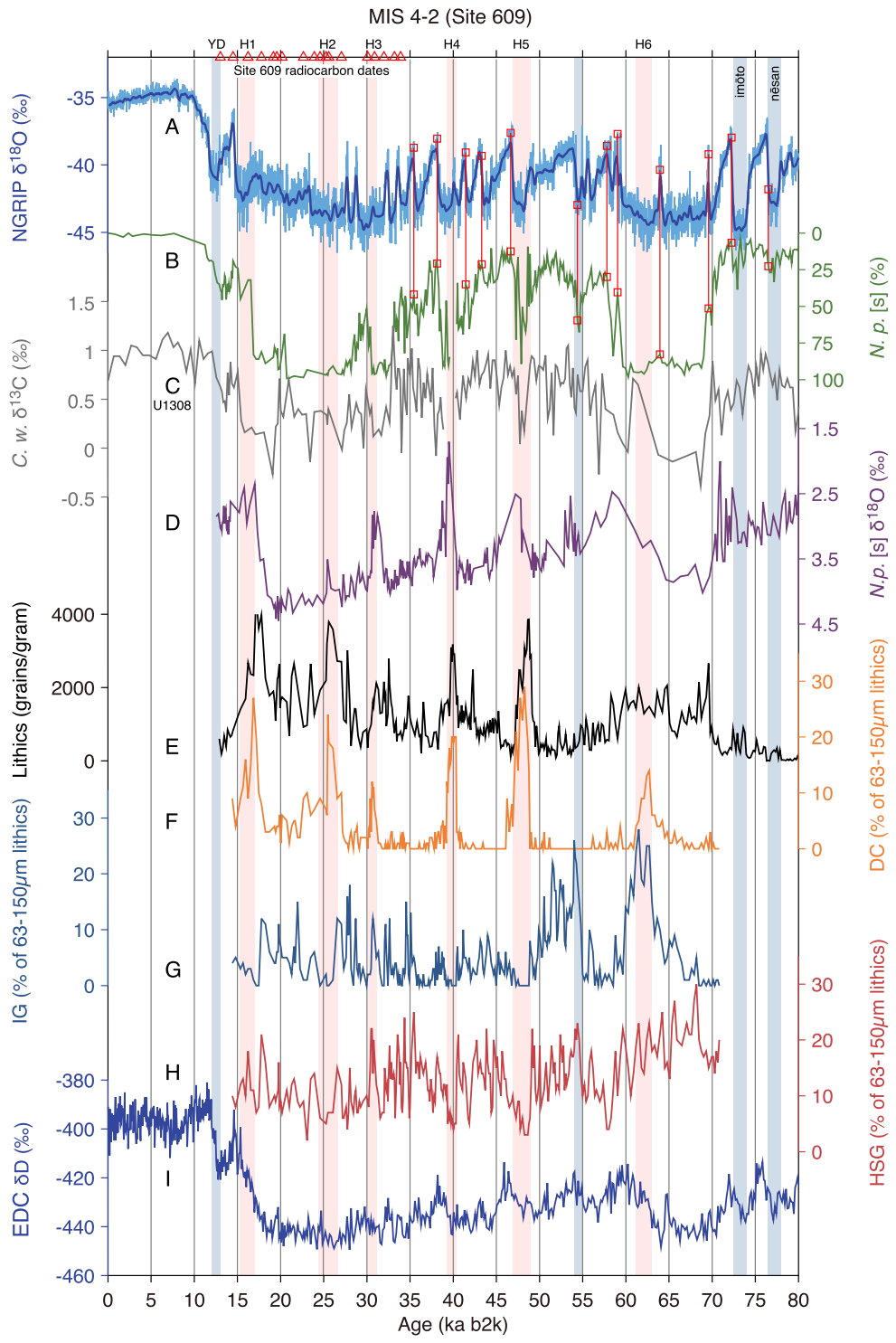

Fig. 2. Site 609 record from MIS 4–2 (Bond et al., 1999) with radiocarbon dates (red triangles) and GICC05 model-extended tie points (red squares) (Obrochta et al., 2012). A) North GRIP ice core δ^{18}O (Andersen et al., 2004), B) *N. pachyderma* [s] percentage (green), C) Site U1308 benthic *C. wuellerstorfi* δ^{13}C (gray; Hodell et al., 2008), D), *N. pachyderma* [s] δ^{18}O (purple), E) >150 μm lithic grain concentration (black), F) detrital carbonate (DC; orange), G) Icelandic glass percentage (IG; blue), H) hematite-stained grain percentage (HSG; red), and I) EPICA Dome C ice core δD (Jouzel et al., 2007) using the AICC2012 chronology (Veres et al., 2013). DC, IG, and HSG are percentages of 63–150 μm lithic fraction. Orange vertical bars denote Heinrich Events, and blue bars non-Heinrich cold stadials. (For interpretation of the references to color in this figure legend, the reader is referred to the web version of this article.)

IRD deposited during Heinrich Events H1 to H6 (Bond et al., 1992), and results from Site 609 were the first to demonstrate a link between North Atlantic sea surface temperature (SST) and Greenland air temperature (Bond et al., 1993), leading to the observation that progressively cooler Greenland insterstadials were bundled between Heinrich Events ("Bond Cycle"). Results from Site 609 further demonstrated that each of these Heinrich Events was preceded by increased lithic flux with high proportions of HSG and fresh, unweathered IG (Bond and Lotti, 1995; Bond et al., 1999).

At Site 609, peak lithic grain concentrations occur within intervals of high abundance of the planktic polar foraminifer *N. pachyderma* [s], indicating cold surface conditions. As lithic content

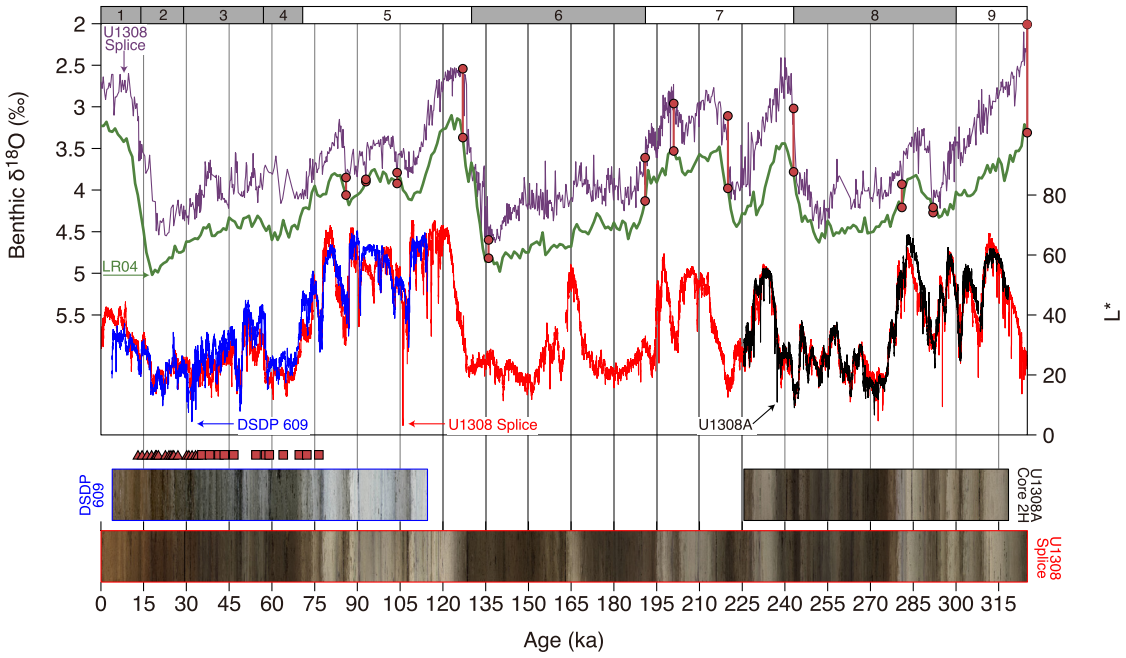

Fig. 3. Site 609 and Hole U1308A were aligned to the U1308 post-cruise, modified composite splice using sediment lightness (L^*) records. L^* was calculated from the core photograph for Site 609 (blue) and from the U1308 shipboard line-scanner images for the modified splice (red) and U1308A (black). The age model used in this study is based on alignment of U1308 benthic *C. wuellerstorfi* δ^{18}O (purple) to the LR04 benthic isotope stack (green; Lisiecki and Raymo, 2005) from MIS 9 to late MIS 5 (top). The younger interval uses the latest Site 609 age model (Obrochta et al., 2012) consisting of recalibrated radiocarbon dates (triangles) and GICC05 ages (squares). Modified U1308 splice, benthic δ^{18}O, LR04 age tie points (red circles), and 609 to U1308 depth match points are from Hodell et al. (2008). (For interpretation of the references to color in this figure legend, the reader is referred to the web version of this article.)

increases, planktic δ^{18}O values begin to decrease primarily due to the effects of isotopically light meltwater (but also potentially due to either contamination by fine DC, as pointed out by Hodell and Curtis (2008), or by sea ice formation as suggested by Hillaire-Marcel and de Vernal (2008)). Concurrently, benthic foraminifer δ^{13}C exhibits depleted values, which is consistent with reduced NADW formation compensated by encroachment of southern-sourced waters into the North Atlantic basin.

The Site 609 HSG record was central to the theory that a "1500-yr" pacing underlies and sets the D–O Event tempo (Bond et al., 1997) and triggered much discussion of periodic suborbital climate change. Subsequent work to modernize the Site 609 age model (using the Marine09 radiocarbon calibration and GICC05 model-extended chronology; Fig. 2A, 2B) showed that HSG at this site is not characterized by a single 1500-yr cycle but is more consistent with distinct 1000 and 2000-yr components (Obrochta et al., 2012).

3. Materials and methods

3.1. Stratigraphic correlation

The uppermost ~8 m of Site 609 (representing the last ~115 ka) has been synchronized to the Site U1308 modified composite splice (Hodell et al., 2008), as shown in Fig. 3. We calculated color reflectance (e.g., $L^*a^*b^*$; Ortiz et al., 1999) values from red, green, and blue (RGB) channel data extracted from the Site 609 core photograph (Ruddiman et al., 1987) and the Site U1308 shipboard core line-scanner images (Expedition 303 Scientists, 2006) along the modified composite splice (0–21.56 mcd), as well as from Core U1308-2H over the interval 11.94 to 18.37 mbsf, which is not in the Site U1308 composite splice but preserves a sedimentary record spanning early MIS 7 to late MIS 9. The shipboard spectrophotometer color reflectance data (2-cm resolution) correlate well with the line-scanner color reflectance data used here ($L^*R^2 = 0.95$; Supplemental Fig. 1). The much higher resolution (0.01 cm) line-scanner reflectance data were required to precisely align Core U1308A-2H to the modified composite splice.

3.2. Age model

The Site 609 age control points (Fig. 2) were transferred to Site U1308 (Fig. 3), incorporating recent refinements (Obrochta et al., 2012). These improvements are 1) inclusion of eleven additional radiocarbon dates that were previously uncalibrated (Bond et al., 1993; Elliot et al., 1998), 2) usage of the Marine09 radiocarbon calibration curve (Reimer et al., 2009) with a constant 405 yr reservoir correction, and 3) optimized correlation of the % *N. pachyderma* [s] ties (Bond et al., 1999) to the virtually-complete North GRIP (NGRIP) ice core with the GICC05 model-extended chronology (Rasmussen et al., 2006; Svensson et al., 2008; Wolff et al., 2010). Our age model uses radiocarbon dates from 13 to 34 ka, ties to NGRIP from 35 to 76 ka, and correlation of the U1308 benthic δ^{18}O record to the LR04 δ^{18}O stack (Lisiecki and Raymo, 2005) from 86 to 325 ka. The LR04 tie points used here are from Hodell et al. (2008).

The resulting average sedimentation rates are 7.1 cm/ky for MIS 4–2, 4.4 cm/ky for MIS 6, and 7.3 cm/ky for MIS 8. At 1-cm sampling, this produces an average resolution of ~180, 230, and 150 yr, respectively. The results of spectral analysis are, of course, highly dependent on the quality of the age models.

3.3. Grain abundance analysis

The abundance of HSG, IG, DC, *N. pachyderma* [s], and bulk lithics (Fig. 4) was determined from U1308 material within the MIS-6 and 8 intervals. To perform these counts the modified splice was sampled by taking half-round slices (~10 cc) at a 1-cm interval from 8.84 mcd to 11.55 mcd, corresponding to MIS 6. Core U1308A-2H was sampled with 5 cc scoops a 1-cm resolution from 12.88 mbsf to 17.62 mbsf (14.94–20.05 mcd). Bulk lithic, DC, and foraminifer counts were performed at an average 2-cm interval

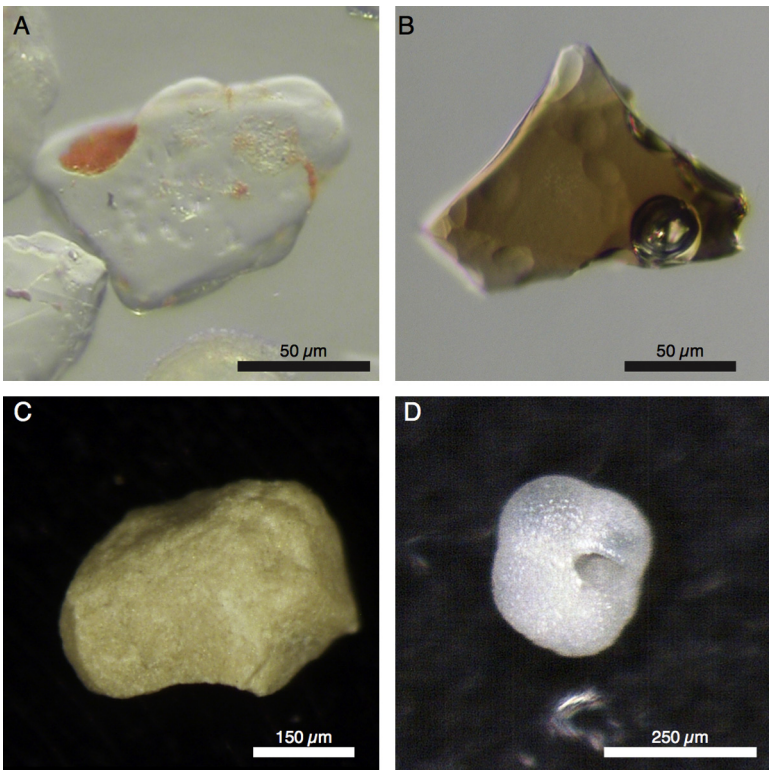

Fig. 4. Photomicrographs of the primary sediment types used in the study. From grain-mount slides (63–150 μm) are A) a hematite-stained quartz grain and B) an Icelandic glass shard, and from loose sediment (>150 μm) are C) detrital carbonate, and D) *N. pachyderma* [s].

on loose sediment from the >150 μm fraction using a reflected light microscope. HSG and IG counts were performed at a 1-cm interval on the 63–150 μm size fraction using grain mount slides. Accurate counts of HSG in the MIS-6 interval required carbonate digestion due to the increased abundance of foraminifers. Therefore 63–150 μm DC counts are limited to the MIS-8 interval.

Because sample weights are not available for Core U1308-2H, grain concentration for key intervals is estimated based on the volume and weight of samples from corresponding composite depths in the modified splice. These are ∼20-cc, half-round continuous 2-cm slices.

Counts of the 63–150 μm fraction were performed with a petrographic microscope, as described by Bond et al. (1997). The sample was illuminated with an external fiber optic light source with a white reflector placed over the microscope's condenser. Adjusting the height of the reflector relative to the stage allows for a position to "be found that creates a strong impression of relief and brings into striking view details of surface textures and coatings on grains" (Bond et al., 1997).

3.4. Spectral analysis

Spectral analysis of HSG was performed by multitaper method (MTM) using the software package SSA-MTM Toolkit (Ghil et al., 2002). HSG was first interpolated to an even 240-yr and 150-yr step for MIS 6 and 8, respectively. MTM analysis of MIS 8 HSG was limited to the interval from 300 to 260 ka.

3.5. Elemental analysis

A total of 64 individual DC grains from MIS 8 and 4–2 were measured for Mg/Ca and Sr/Ca ratios to determine whether they appear derived from the same population and therefore likely of similar provenance. Grains from the MIS 8 interval were measured by laser ablation inductively coupled plasma mass spectrometry (LA-ICP-MS) at the University of Tokyo Atmosphere and Ocean Research Institute. Grains from the MIS 4–2 interval were measured by inductively coupled plasma atomic emission spectrometry (ICP-AES) at the University of Cambridge Department of Earth Sciences.

3.5.1. ICP-AES

Five individual DC grains were picked from each of the H1, H2, H4, and H5 intervals in the U1308 splice for analysis at the University of Cambridge, Department of Earth Sciences using a Vista ICP-AES. For H1, H2, H4, and H5, grains were picked from samples U1308C-1H-1W 92–94 cm (0.92 mcd), U1308C-1H-1W 130–132 cm (1.30 mcd), U1308C-1H-2W 116–118 cm (2.66 mcd), and 1308E-1H-2W 70–72 cm (3.52 mcd), respectively. Prior to analysis, samples were diluted in 0.1M HNO_3 to obtain a Mg concentration of ∼0.3 ppm. Calibration of calcium, magnesium, and strontium was performed with mixed standard solutions (Greaves et al., 2005).

3.5.2. LA-ICP-MS

Individual DC grains (Supplemental Fig. 2) were picked from each of the three MIS-8 DC deposition events (labeled 8.1, 8.2, and 8.3 by Channell et al., 2012) for LA-ICP-MS analysis using a Resonetics Resolution M-50 ablation system attached to a Thermo Element XR ICP-MS. For the 8.1 event (∼243 ka) 15 grains were picked from sample U1308A-2H-4W 8–9 cm (13.18 mbsf). For the 8.2 event (∼249 ka), 9 grains were picked from sample U1308A-2H-4W 54–55 cm (13.64), 3 grains from 57–58 cm (13.67 mbsf), and 4 grains from 58–59 cm (13.68 mbsf). For the 8.3 Event (∼263 ka), 13 grains were picked from U1308A-2H-5W 4–5 cm (14.64 mbsf).

Laser energy was 50 mJ with a spot beam. Beam width was set to 155 μm for most analyses but reduced to 112 μm for grains less than ∼500 μm. Beam width was kept constant during individual runs. Continuous ICP-MS measurements were made for each run using triple detection and low resolution settings, and mass

offset was determined at the start of each day of analyses. Up to 10 individual grains of similar size were analyzed during each run with constant beam size. Prior to grain ablation, background values were measured for ~3 min, and standards JCp-1 and NIST-614 were measured along a line for 5 min each at a speed of 5 μm/s. Grains were held stationary and ablated for 120 s, with 60 s of equilibrium time between each grain measurement. Measured intensities were background subtracted and drift corrected. The mean intensity of ^{24}Mg, ^{43}Ca, and ^{88}Sr was calculated for each grain after discarding the initial and final ~2 s. When the laser fully broke through a grain, the corresponding values were discarded. The mean ablation time from which intensity was calculated is 96 s with a range of 46 to 116 s. NIST-614 was used to calibrate the results presented here. Calibration with JCp-1 yielded similar results.

One grain with moderate Mg/Ca ratios (0.42 mol/mol) was selected from the 8.2 DC event from sample U1308A-2H-4W 57–58 cm for higher resolution measurements. Twenty-nine individual measurements were performed across the grain's surface with a 24 μm spot beam using the same parameters as described above.

3.6. Stable isotopes

Stable isotopes were measured on the planktic foraminifer *N. pachyderma* [s] following the method of Hodell et al. (2008). Specimens were picked from the >212-μm size fraction at a 2-cm spacing within the MIS-6 and 8 intervals of the U1308 modified splice. Analyses were performed using a Finnigan MAT 252 mass spectrometer at the University of Florida, Department of Geological Sciences.

4. Results

New grain abundance data and planktic *N. pachyderma* [s] δ^{18}O from Site U1308 are shown in Fig. 5 together with the previously published benthic *C. wuellerstorfi* δ^{13}C record (Hodell et al., 2008). Note that (with the exception of lithic grain concentration) the vertical axes of individual panels presenting the same proxy are identically scaled in order to highlight the differing amplitudes of variability during each glaciation, and the horizontal axes cover an identical time range (80 ky). Elemental analyses of individual DC grains are shown in Fig. 6. Data reported here are available at http://dx.doi.org/10.1594/PANGAEA.834640.

4.1. Iceberg and sea ice rafted debris

With the exception of IG, the lithic grains at Site U1308, including HSG, are interpreted to primarily reflect iceberg-rafted debris, i.e., IRD. While the primary source for HSG was the Gulf of St. Lawrence during the last glaciation (Bond and Lotti, 1995; Bond et al., 1999), HSG was likely derived from a wider area and transported by sea ice during the Holocene and perhaps other long interstadials (Bond et al., 1997, 1999, 2001). Regarding IG, Kuhs et al. (2014) concluded that >150 μm shards deposited at Site U1304 (53°03′N, 33°32′W) were likely iceberg-rafted based on generally large size, geochemical heterogeneity, and association with high concentrations of other lithic grain types. At Site U1308, however, we observe a less consistent relationship between fresh, non-weathered and transparent IG content and total lithic concentration, particularly in the 63–150 μm fraction (Fig. 5).

North Atlantic sea ice distribution is sensitive to changes in wind stress, which is in turn affected by the presence and configuration of the LIS (Manabe and Broccoli, 1985; Oka et al., 2012). We therefore feel it is likely that both icebergs and sea ice contributed IG to Site U1308, and the relative importance of each process may vary with differing oceanographic conditions between the discrete glacial intervals studied, as well as within the same glaciation. For example, HSG and IG covaried within MIS 4–2 (Fig. 2G, 2H), suggesting a similar delivery mechanism, but IG is decoupled from other lithic grain types throughout much of MIS 8 and 6 (Fig. 5). Within the MIS-6 interval in particular, peak IG content is more consistently associated with high total foraminifer abundance, especially *N. pachyderma* [s], which is associated with sea ice and brine (e.g., Hillaire-Marcel and de Vernal, 2008, and references therein). IG could be entrained as atmospheric fallout and delivered to the site as the sea-ice margin expanded south of Iceland. Coastal sea ice formation can directly incorporate seafloor sediment, and in this case the rafted shards could exhibit geochemical signatures associated with multiple Icelandic volcanic provinces.

4.2. MIS 8

Results from MIS 8 (Fig. 5B) are comparable to those of the last glaciation (Fig. 2; Section 2.2), with abrupt, high-amplitude variations in all measured proxies. Each interval of increased *N. pachyderma* [s] abundance is associated with elevated IRD content. Prior to Termination III (~243 ka), lithic grain and *N. pachyderma* [s] abundance is consistently positively correlated ($r = 0.64$, $p < 0.0001$). Benthic δ^{13}C exhibits high-amplitude fluctuations (−0.65‰ to 1.28‰), with a mean of 0.26 ± 0.36 (1σ), and consistently tracks both lithic ($r = -0.41$, $p < 0.0001$) and *N. pachyderma* [s] abundance ($r = -0.65$, $p < 0.0001$). *N. pachyderma* [s] comprises as little as ~1% to as much as 95% of the planktic foraminifer assemblage, and late-glacial (<275 ka) changes in abundance are rapid, occurring in less than 1000 yr. At ~249 ka, *N. pachyderma* [s] abundance increases from ~30% to 90% in ~850 yr, then returns to 30% in ~1000 yr.

Four distinct, IRD events occur within the latter portion of MIS 8 at ~275, 263, 249, and 243 ka (8.4–8.1 events), the younger three of which are characterized by high DC content. Light planktic δ^{18}O excursions up to a 1.3‰ magnitude follow the onset of glacial IRD events. Estimates of lithic grain concentration suggest an increase of ~1000 to 2500 grains/g above the near-zero (<20) ambient levels during the 8.3, and 8.1 DC events, and these are directly preceded by "precursor" increases in siliceous IRD, HSG and IG, similar to the last glacial HS Heinrich Events (H1, H2, H4, and H5; Fig. 2E–H) (Bond and Lotti, 1995; Bond et al., 1999). While onset of the 8.4 and 8.3 IRD events coincides with high *N. pachyderma* [s] abundance, lithic grains reach over 99% of the >150 μm fraction and planktic foraminifers are virtually absent. *N. pachyderma* [s] abundance decreases during a brief reduction in IRD input early in the 8.4 event. The 8.1 DC event and H1, which occur during glacial terminations, are characterized by intermediate to low *N. pachyderma* [s] abundance.

Mg/Ca and Sr/Ca of individual MIS-8 DC grains from the 8.1, 8.2, and 8.3 DC events suggest they are from the same population as those from the last glacial HS Heinrich Events (Fig. 6A). The high Mg content, up to a 1:1 ratio with Ca, is consistent with the presence of dolomite and a Hudson Strait source. Narrow-beam LA-ICP-MS analysis across the surface of a single grain from the 8.2 event reveals highly variable Mg content (Fig. 6B), likely indicative of heterogeneous dolomitization, perhaps across microfronts.

One distinction between MIS 8 (Fig. 5B) and MIS 4–2 (Fig. 2F) is that, during the former, 63–150 μm-sized DC remains an elevated lithic component for an extended time (up to ~2500 yr) following surface and deep recovery (low *N. pachyderma* [s] abundance and high benthic δ^{13}C). This is observed following the 8.1 and 8.3 DC events but not during 8.2 or any of the last glacial HS Heinrich

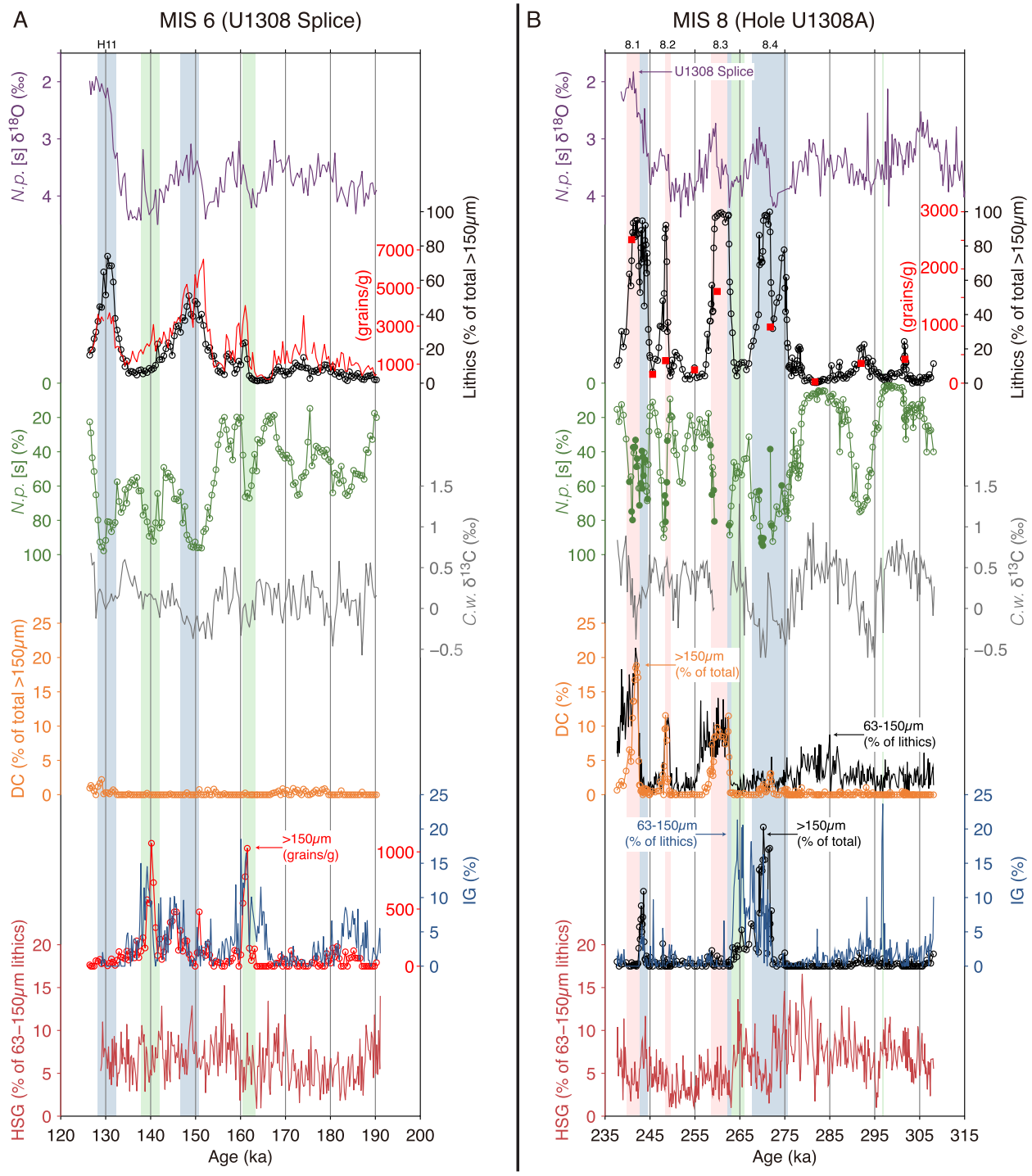

Fig. 5. New results for A) MIS 6 from the U1308 splice and B) MIS 8 from Hole U1308A: planktic *N. pachyderma* [s] δ^{18}O (purple; U1308 splice); >150 μm lithic percent (black, open circles) and concentration (red); *N. pachyderma* [s] percent of total planktic foraminifers (green) for samples with >200 individual foraminifers (open circles) and >100 individuals (filled circles); >150 μm DC percent (orange, open circles) and 63–150 μm percent (gray; MIS 8 only); 63–150 μm percent (blue) with concentration (red, open circles; MIS 6) and percent (black, open circles; MIS 8) from the >150 μm IG; 63–150 μm HSG percent (red). >150 μm data are percent of total fraction, and 63–150 μm data are percent of lithic fraction. Blue vertical bars: >50% lithic grains; light green bars: IG is ~15% of the 63–150 μm fraction; light orange bars: >10% DC. Benthic *C. wuellerstorfi* δ^{13}C (gray) from the U1308 splice are from Hodell et al. (2008). (For interpretation of the references to color in this figure legend, the reader is referred to the web version of this article.)

Events. Bioturbation is unlikely to have transported this material the required ~18 cm up core.

The MIS 8 HSG record exhibits a range in abundance from 1% to 17%, with a mean and standard deviation of 6.2 and 2.8, respectively. With the exception of directly preceding the 8.1 and 8.3 DC events, HSG generally exhibits low abundance during the latter portion of MIS 8, from ~270 ka, perhaps due to dilution by DC. Prior to this, during the mid-glacial interval, from 300–260 ka, HSG exhibits enhanced amplitude variability and identifiable maxima and minima, with midpoints spaced on average 1400 ± 340 yr apart (Fig. 7). A broad spectral peak spans the millennial band from 1/1690 to 1/1360 yr, centered at 1/1500 yr.

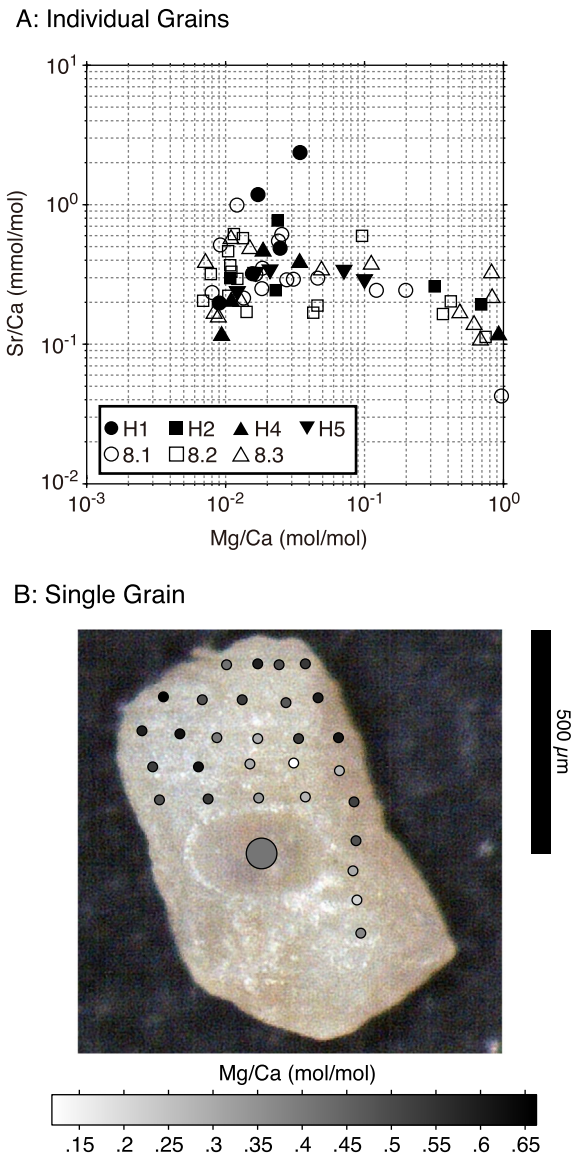

Fig. 6. A) Cross plot of Mg/Ca and Sr/Ca for individual DC picked from MIS 4–2 HS Heinrich layers in the U1308 splice (filled symbols) and from the MIS 8 DC-rich layers in Hole U1308A (open symbols). MIS 4–2 and 8 grains where analyzed by ICP-AES and LA-ICP-MS, respectively. B) Mg/Ca ratios from 25-μm spot LA-ICP-MS measurements across the surface of an individual grain from the 8.2 event (1308A-2H-4W 57–58 cm). Large indention in grain center is from ablation for data used in (A). See Supplemental Fig. 2 for photomicrographs of all grains.

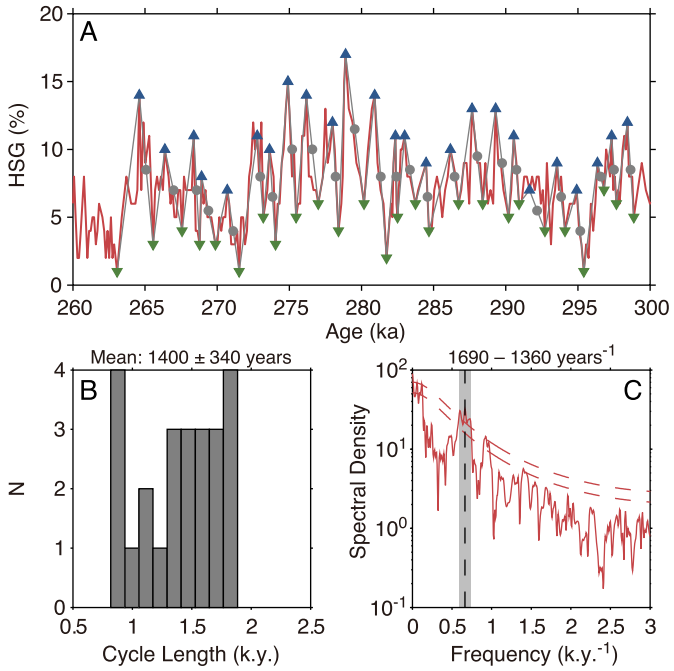

Fig. 7. A) U1308A MIS 8 HSG from 260 to 300 ka showing cycle minima, maxima, and midpoints. B) Histogram of elapsed time between cycle midpoints (~1400 ± 340 yr mean). C) MTM power spectrum showing a wide, 99%-confident spectral peak centered at a 1/1500 yr frequency (dashed line). Shaded region denotes the range of 99% confidence (1/1690–1/1360 yr).

4.3. MIS 6

Lithic results from MIS 6 (Fig. 5A) exhibit pronounced differences from those of MIS 8 and the last glaciation. While there are light planktic δ^{18}O excursions of similar magnitude as the surrounding glaciations, these are not associated with intervals dominated by lithic grains. Planktic foraminifer abundance remains high throughout the entire MIS 6 glaciation, and the maximum lithic grain abundance is less than 75% of the >150 μm fraction. The concentration of lithic grains, however, is nearly continuously elevated, with background levels rarely below 1000 grains/g.

Intervals of peak lithic concentration do not correspond to intervals of particularly high lithic percentage. During the earliest (~175 ka) of four distinct MIS-6 lithic deposition events, lithic content comprises only 15% of the >150 μm fraction but exceeds 3500 grains/g, a similar concentration as during the last glacial HS Heinrich Events. The event from 161 to 156 ka is similarly characterized by low lithic percentage (<25%) and high concentration (~4000 grains/g). The maximum concentration of >6500 grains/g occurred at ~151 ka, during an extended interval of lithic deposition, lasting for ~15 ky and centered on 146 ka, but lithics only comprise at most ~50% of the >150 μm fraction at this time. While H11 exhibits the highest percentage of lithic grains (74%), it is characterized by relatively low concentration that averages ~ 3500 grains/g.

There also appears to be less surface-deep coupling at this site during MIS 6. While the correlation of *N. pachyderma* [s] abundance with lithic percentage ($r = 0.64$, $p < 0.0001$) and with concentration ($r = 0.64$, $p < 0.0001$) is significant and comparable to the other glaciations, benthic δ^{13}C is not highly correlated with any of these parameters. Correlation coefficients are: $r = -0.32$ ($p < 0.001$) for *N. pachyderma* [s], $r = -0.21$ ($p < 0.05$) for lithic percentage, and $r = -0.34$ for lithic concentration ($p < 0.0001$). Benthic δ^{13}C exhibits, on average, lighter (0.11‰) and less variable (0.24; 1σ) values than during MIS 8 (0.26 ± 0.36‰) and 4–2 (0.52 ± 0.30‰), with no extended intervals heavier than 0.6‰. For comparison, the last glacial interstadials at this location exhibited values typically exceeding 0.95‰ (Fig. 2C).

The cold phases at ~184 ka and ~140 ka are not distinguished by high total lithic percentage or concentration. Lithic grains in these intervals are primarily IG, with both the older and younger intervals characterized by increased relative abundance (proportion of lithic fraction) of 63–150 μm IG. The cold period at ~140 ka is also marked by high IG concentration (~1000 IG grains/g). Periods of increased IG occur at ~20 ky intervals, i.e., the cold event at ~162 ka is also marked by high IG abundance and concentration.

N. pachyderma [s] variations suggest that MIS 6 was characterized by two distinct phases (e.g., Margari et al., 2010). *N. pachyderma* [s] is relatively abundant throughout the entire glaciation (15–98%); during the early glacial from ~190–155 ka, *N. pachyderma* [s] abundance averages ~20% during warm periods and increases to ~65% during cooler phases. Subsequent to ~155 ka, the record exhibits a baseline shift to higher abundance, indicating

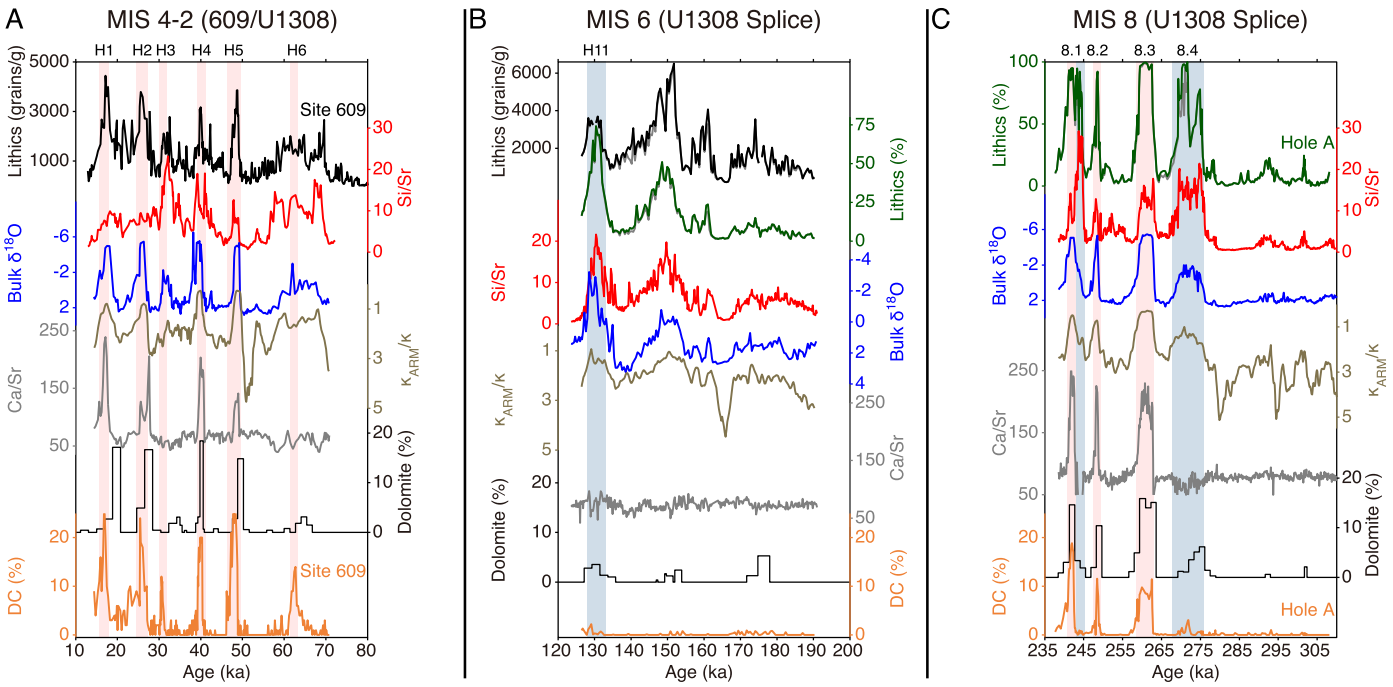

Fig. 8. Lithic content proxy data from the U1308 splice section compared to petrologic count data for A) MIS 4–2 from Site 609, B) MIS 6 from the U1308 splice, and C) MIS 8 from U1308A. Proxy data are Si/Sr ratio (red), bulk δ^{18}O (blue), magnetic grain size (κ_{ARM}/κ; brown), Ca/Sr (gray), and XRD-based dolomite percentage (Ji et al., 2009; black). Grain count data are lithic concentration (black) and percent (green) and DC percent (orange). For B and C, non-IG lithic concentration and abundance (gray) are also shown. All abundance data are percent of total >150 μm fraction. Lithic percent is unavailable for MIS 4–2, and lithic concentration is unavailable for MIS 8. Orange vertical bars show high DC events; blue vertical bars show siliceous IRD events. (For interpretation of the references to color in this figure legend, the reader is referred to the web version of this article.)

generally colder conditions with more severe cold events. Maximum abundance reaches ~95% but decreases to only ~50% during intervening warmings, which is the same relative magnitude as during the early glacial (and substantially less than that of MIS 8). In addition, both warm-to-cold and cold-to-warm transitions are less abrupt than during the surrounding two glaciations, exhibiting a typically 4000-yr duration. This four-fold increase relative to MIS 8 is too large to be entirely explained by lower sedimentation rate/sampling resolution.

The MIS 6 HSG record exhibits a similar range, mean, and standard deviation (1–15%, 6.3 and 2.5, respectively) as the MIS 8 record. However, it does not exhibit clear, visually apparent "cycles" (though it does contain one 99%-confidence spectral peak at 1/950 yr; Supplemental Fig. 3).

5. Discussion

5.1. Heinrich events prior to the last glacial

Hudson Strait-derived material is distinguishable from other sources of North Atlantic sediment by a Paleozoic dolomitic limestone component with highly depleted δ^{18}O (~−5‰; Hodell and Curtis, 2008), relatively low Sr content (Hodell et al., 2008), and a distinctive biomarker signature (Naafs et al., 2011). The particular nature of this material has allowed the development of a number of proxies for HS Heinrich-like events (Hodell and Curtis, 2008; Hodell et al., 2008; Ji et al., 2009; Stein et al., 2009; Naafs et al., 2011; Channell et al., 2012; Channell and Hodell, 2013; Naafs et al., 2013). Results generally indicated that HS Heinrich-like layers are prominent features of all "100-ky world" glaciations (back to MIS 16), except for MIS 6.

Until now, these proxies were only calibrated for the last glaciation. Our results both extend the directly-calibrated interval through MIS 8 and confirm the evidence for virtual absence of sand-sized DC in the MIS-6 interval at Site U1308 (Fig. 8). DC concatenated over all three glaciations exhibits high correlation with bulk δ^{18}O ($r = 0.64$, $p < 0.001$; $n = 594$), split-core XRF Ca/Sr ($r = 0.59$, $p < 0.001$; $n = 594$), and magnetic grain size (κ_{ARM}/κ; $r = 0.47$, $p < 0.001$; $n = 594$). Last glacial HS Heinrich Events are all expressed as peaks in Ca/Sr exceeding 150, as are the 8.1–8.3 DC events. However, magnetic grain size (κ_{ARM}/κ) and bulk δ^{18}O are not strictly a proxy for Hudson Strait-derived DC. Both κ_{ARM}/κ and bulk δ^{18}O are highly correlated to total lithic percent during MIS 6 ($r = -0.66$, $p < 0.001$ and $r = -0.84$, $p < 0.001$ respectively), and each exhibits a significant response to IRD events within intervals lacking dolomite and DC.

We also show that individual DC grains deposited during the MIS 8 DC events exhibit an identical geochemical signature to those from the last glacial HS Heinrich Events, indicating similar provenance. This implies that these three DC IRD events (8.3, 8.2, and 8.1) represent surging of the LIS in the Hudson Strait region, constituting true HS Heinrich Events at ~263, ~249, and ~243 ka. Similar to the last glaciation, 8.1 and 8.3, the larger of the three in terms of lithic grain concentration (2500 and 1600 grains/g, respectively) are directly preceded by "precursor" IRD events (Bond and Lotti, 1995; Bond et al., 1999), with HSG, IG, and bulk lithics all peaking directly before the HS Heinrich Event. This is consistent with an external trigger for Heinrich Events. Conversely, the so-called H11 event during TII (~130 ka) does not appear to be associated with either precursor events or with large-scale surging from the HS region, and has very low Ca/Sr and dolomite content at Site U1308 (Fig. 8B).

5.2. Nature of variability during the past three glaciations

5.2.1. Implications of HSG variations

The HSG records reported here are the first published after the pioneering investigations of Bond and Lotti (1995) and Bond et al. (1997, 1999, 2001), as well as the first reported for time periods prior to the last interglacial (MIS 5). The MIS 8 HSG results (Figs. 7

and 5B) are similar to those of the last glaciation (Fig. 2H) in that both records exhibit broadly comparable down-core variability and pacing, particularly within mid-glacial intervals of intermediate ice volume, that become less pronounced as each glacial maxima is approached (~250–240 ka; ~30–20 ka). The MIS 4–2 HSG record exhibits a mean elapsed time between cycle midpoints of ~1570 ± 700 yr, and the most significant spectral frequency is a broad peak centered at 1/1390 yr (Obrochta et al., 2012; Supplemental Fig. 4). This resembles MIS 8 results in both cycle length (~1400 ± 340) and frequency (1/1500 yr).

Cycle lengths within the radiocarbon- and GICC05-dated portion of the MIS 4–2 HSG record are bimodally distributed and primarily comprised of ~1000 and ~2000 yr components (Obrochta et al., 2012). This is less apparent in MIS 8, which lacks precise millennial-scale age control. The relatively invariable sedimentation rates inherently produced by our orbital scale age model, for which no alternative is currently available, may be unrealistic due to occurrence of HS Heinrich Events, particularly during late MIS 8. Although the apparent cyclicity observed in HSG is within the mid to early glacial interval that lacks major lithic deposition events, statistical durations and frequencies should be interpreted with caution. We note that the pacing of the MIS 8 and 4–2 HSG records is generally similar.

The MIS 6 HSG record (Fig. 5), on the other hand, shares little similarity with those of the surrounding glaciations. Relatively high-amplitude depositional events are spaced at much longer intervals, approximately 4 to 8 ky, which is similar in scale to the typically longer-duration cold events reported from the Iberian Margin during MIS 6 (Margari et al., 2010). Also, unlike the MIS 8 and 4–2 HSG records, there is no significant spectral peak at a frequency that corresponds to this mean pacing. Mathematically, there is one 99%-confidence spectral peak at an approximate 1/950-yr frequency (Supplemental Fig. 3). While this is the same frequency at which the stacked Holocene HSG record is coherent with cosmogenic ^{14}C and ^{10}Be production (Bond et al., 2001; Obrochta et al., 2012), it could simply reflect the 240-yr sampling step ($4 \times 240 = 960$) in a noisy record.

HSG variability was originally suggested as both a precursor to HS Heinrich Events and to be a pacemaker for D–O Events (Bond and Lotti, 1995; Bond et al., 1997, 1999). While increasing HSG consistently precedes all HS Heinrich Events including 8.1 and 8.3, the linkage between ice-rafted HSG and D–O Events through freshwater forcing is tenuous. No systematic relationship exists between HSG peaks and Greenland climate. Even with the age model used here, the most precise available for this site during MIS 4–2, there is no consistent phase relationship between HSG and NGRIP ice core δ^{18}O. The association was primarily based on a common 1470-yr period, but recent work shows that little evidence exists for actual 1500-yr intervals of climate variability in either Greenland records (Ditlevsen et al., 2007) or the HSG record from well-dated intervals of Site 609 (Obrochta et al., 2012). Regardless of forcing, if HSG variability is in some way causally linked to North Atlantic regional climate change, any potential forcing would have been less of a factor during MIS 6 than during MIS 8 and 4–2.

5.2.2. Global connections to North Atlantic variability

Detectable sea level increase at far-field locations indicates a measurably large ice mass loss of up to 15 m sle (sea-level equivalent) during the HS Heinrich Events of the last glaciation (Yokoyama et al., 2001a, 2001b). Early modeling results suggested that such a large amount of freshwater would have greatly affected North Atlantic hydrography (Manabe and Stouffer, 1988), decreasing North Atlantic deepwater (NADW) formation. This is consistent with the strong coupling between IRD events, cold surface conditions, and depleted benthic δ^{13}C observed at this site during MIS 4–2 (Fig. 9B–E). Consistent with "bipolar see-saw" theory, as proposed by Crowley (1992), northward heat flow was reduced, resulting in Antarctic warming (Blunier and Brook, 2001; EPICA Community Members, 2006; Veres et al., 2013; e.g., EDC δD; Fig. 9I).

Further observational evidence for this interhemispheric phasing is provided by Iberian Margin records that exhibit benthic δ^{18}O similar to Antarctic ice cores (Shackleton et al., 2000), decreased grain size along deepwater routes that suggests slower circulation (McCave et al., 1995; Hall and McCave, 2000), and increased ^{14}C reservoir ages at upwelling sites that indicate slower meridional overturning circulation (Kubota et al., 2014). Southward displacement of circulation belts, most likely due to cooling and sea ice expansion (e.g., Denton et al., 2010), is indicated by altered precipitation patterns in South America (Wang et al., 2004; Kanner et al., 2012; Cheng et al., 2013; Nace et al., 2014), Africa (Weldeab et al., 2007), Asia (Wang et al., 2001), and Australia (Muller et al., 2008; Mohtadi et al., 2011), as well as Antarctic upwelling (Anderson et al., 2009) and deep-ocean ventilation (Ahn and Brook, 2007, 2008).

Results presented here indicate a similar series of events likely occurred during MIS 8. Considering that the Site U1308 age model for MIS 8 is orbital in scale and cannot resolve the expected changes in sedimentation rate associated with HS Heinrich Events, Antarctic air temperature increase (Jouzel et al., 2007; Bazin et al., 2013) corresponds in general to the timing of high IRD deposition, high *N. pachyderma* [s] abundance, and depleted benthic δ^{13}C (Fig. 9C, 9D, 9E, 9I). This suggests that the hydrographic changes during the MIS-8 HS Heinrich Events may have been comparable to those that occurred during the last glaciation. While East Asian monsoon intensity (Fig. 9H) appears controlled primarily by high-amplitude Northern Hemisphere insolation changes (Fig. 9G), brief low intensity events (high δ^{18}O) also correspond to intervals of enhanced DC deposition.

During MIS 6, however, these same proxies indicate a nearly continuous, low-level input of glacial meltwater, a greater influence of orbital precession, and perhaps muted D–O variability. NADW production appears to have been generally reduced (or shoaled) and preconditioned for Heinrich-like reorganization that was ultimately triggered by comparatively weak forcing (e.g., due to a lower disruption threshold, Margari et al., 2010). Benthic δ^{13}C is on average more depleted and does not reach sustained, high values typical of interstadials at this site (~0.95‰), and warm/cool oscillations are lower amplitude and less abrupt. There are very high background concentrations of siliceous IRD (~1000 grains/g) that rarely drop to the near-zero levels characteristic of MIS 8 and 4–2 interstadials, and the highest concentrations occur during high 65°N north insolation (Fig. 9D, 9G), suggesting a connection between ice sheet instability and high summer insolation (Timmermann et al., 2010). MIS 6 IRD results are consistent with model simulations that imply high background IRD with low relative abundance is associated with weaker D–O cycles (Marshall and Koutnik, 2006).

The three intervals of low insolation (high precession) at ~184, ~162, and ~140 ka are characterized by high IG and *N. pachyderma* [s] abundance (Fig. 9B, 9F, 9G). (Only at ~162 ka was there an appreciable increase in the concentration of non-IG lithic grains, though IG still accounts for a large percentage of the 63–150 μm fraction and one third of the total >150 μm lithic grain concentration.) Corresponding to each increase in IG, speleothem δ^{18}O from China (31°N) indicates weakening of the East Asian monsoon (Wang et al., 2008; Fig. 9H), and renewed speleothem and travertine growth in northeastern Brazil (10°S) reflects increased precipitation (Wang et al., 2004), both of which are consistent with a southward displacement of the ITCZ.

If IG reaching Site U1308 is indeed primarily sea-ice rafted, then sea ice expansion over deepwater formation sites may have been the final trigger for reorganizations during times of low

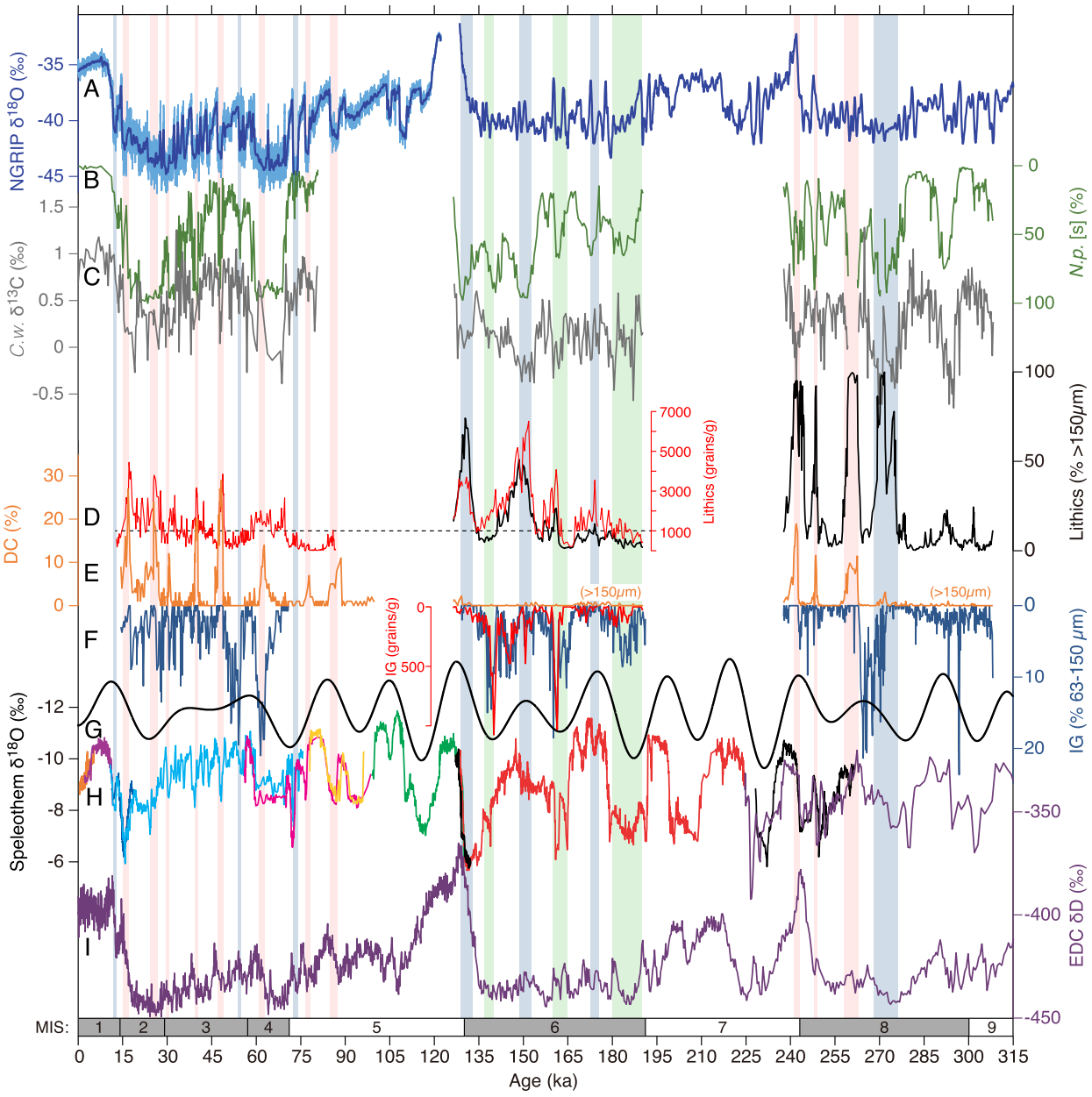

Fig. 9. Combined Site 609/U1308 records are: B) *N. pachyderma* [s] percent (green), C) *C. wuellerstorfi* δ^{13}C (gray), D) >150 μm lithic concentration (red) and percent of total fraction (black), E) DC percent of 63–150 μm fraction (MIS 4–2) and percent of total >150 μm fraction, and F) IG percent of 63–150 μm fraction and >150 μm concentration (MIS 6 only). MIS 4–2 DC extended with V23-81 data from 70.9 to 100 ka after conversion to GICC05 (Obrochta et al., 2014). Also shown are A) North GRIP ice core δ^{18}O (Andersen et al., 2004) extended with the Barker et al. (2011) synthetic record (speleothem chronology), G) 65°N summer insolation, H) Chinese speleothem δ^{18}O (Wang et al., 2001, 2008; Cheng et al., 2009), and I) EPICA Dome C ice core δD (Jouzel et al., 2007) using the AICC2012 chronology (Bazin et al., 2013; Veres et al., 2013). Light blue, green, and orange vertical bars denote IRD, IG and DC events, respectively. (For interpretation of the references to color in this figure legend, the reader is referred to the web version of this article.)

insolation in MIS 6. Generally increased sea ice during MIS 6 is consistent with the high abundance of the ostracode *Acetabulastoma*, commonly known as a "sea ice indicator" in the modern Arctic Ocean, observed on the Rockall Plateau in Core M23124 (Didié and Bauch, 2000). Preconditioning by low-level background meltwater input, as evidenced by consistently high concentrations of IRD, is supported by results from Core V28-82 (Downing, 2008). V28-82 is proximal to Site U1308 and records a nearly identical IRD record, in terms of both lithic grain abundance and concentration, during MIS 6. Excess ^{230}Th measured on V28-82 reveals that the only substantial increase in mass flux occurred during H11. Increased mass flux above background levels is not observed during any of the high-concentration IRD intervals recorded at V28-82. Regardless of the delivery mechanism for IG to Site U1308, the lack of evidence for a considerable increase in non-IG IRD above background levels indicates that these disruptions at ~184 and ~140 ka were triggered by relatively weak (or well-placed) forcing, as the amount of meltwater obtainable from Iceland is much less than that of the Greenland, European, or North American glaciers.

Low dolomite (Ji et al., 2009) and DC throughout MIS 6 at Site U1308 indicate a larger role for regions outside of the Hudson Strait. For example, light planktic δ^{18}O and high IRD concentration beginning from ~152 ka may be related to a European "Fleuve Manche" discharge (Toucanne et al., 2009; Margari et al., 2014). Though the Hudson Strait region did contribute some meltwater, it is unlikely that major surging events occurred as the calved icebergs reaching Site U1308 contained virtually no sand-sized DC. Site U1302/1303 record DC events, but their presence during

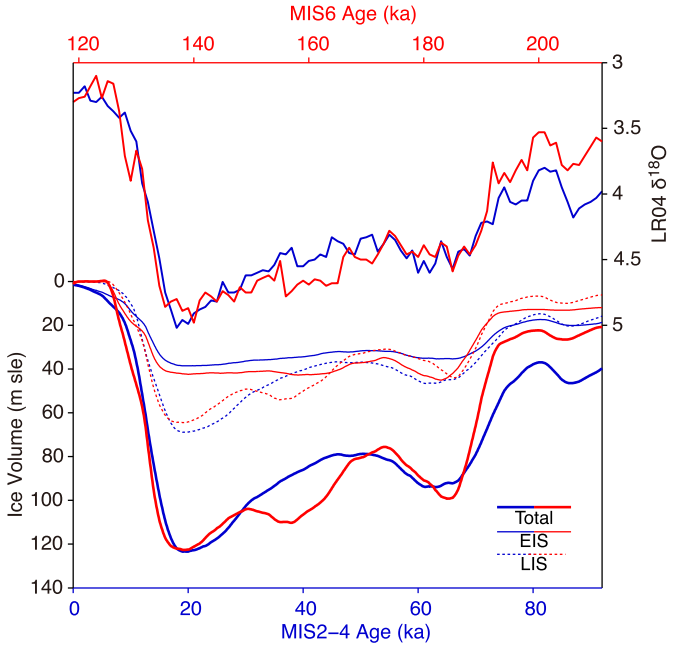

Fig. 10. Comparison of MIS 4–2 records (blue, lower axis) and MIS 6 records (red, upper axis) for A) the LR04 benthic isotope stack (Lisiecki and Raymo, 2005) and B) estimates of total (thick line), Eurasian (thin line), and North American (dashed line) ice volume (Bintanja and van de Wal, 2008). (For interpretation of the references to color in this figure legend, the reader is referred to the web version of this article.)

multiple interglacial stages (MIS 7, 9, 13, 15, and 17) indicates that other processes in addition to ice sheet surging control DC deposition at this location proximal to the LIS (Channell et al., 2012; Channell and Hodell, 2013). Downing (2008) surveyed a number of cores north and south of the IRD Belt but found little evidence for significant DC deposition during MIS 6 at other locations, so it is also unlikely that the locus of deposition changed.

5.3. Implications for MIS 6 ice sheet configuration

The apparent lack of HS Heinrich Events implies differing ice-sheet boundary conditions during MIS 6. Continental geomorphology indicates that both the North American and Eurasian glaciers were configured differently during the penultimate glaciation relative to the last glaciation, though boundaries of the Late Saalian (MIS 6) Eurasian ice sheets are better constrained than those of its North American counterpart (Illinoian). Of the two glacial advances in the Saalian, the earlier Drenthe was greater than the subsequent Warthe (Ehlers et al., 2011). Compiled European data for the period 140–160 ka indicate that the Late Saalian ice sheet's maximum area was significantly larger than that of the Weichselian (MIS 4–2) (Svendsen et al., 2004), though this reconstruction likely reflects a combined representation of both Saalian advances. Through inversion of rebound and sea-level data, the thickness of the Late Saalian ice sheet was estimated to be as much as 4500 m (Lambeck et al., 2006). In North America, Illinoian glacial moraines, dated to MIS 6 by luminescence dating (e.g., Forman and Pierson, 2002), are located farther south than the MIS 2 Wisconsin terminal moraine, suggesting a greater maximum southern ice penetration and perhaps a larger total area, though direct geomorphologic evidence is limited and uncertain.

There is a striking correspondence between the glacial development of MIS 6 and 4–2, with total ice volume evolving similarly, resulting in ~130 m below present sea level at each glacial maxima (e.g., Yokoyama and Esat, 2011) (Fig. 10). Given their current glaciated state, it is reasonable to assume a similar excess ice volume for Greenland and Antarctica during the penultimate and last glacial maxima, which was ~3 and ~20 m sle, respectively (Clark and Mix, 2002). Thus, reconciling an increased MIS 6 Eurasian ice volume would likely require a reduction in North American volume, which is supported by combined geochemical and model results (Bintanja and van de Wal, 2008; Crowley and Hyde, 2008; de Boer et al., 2014; Abe-Ouchi et al., 2013) (Fig. 10). In addition to decreased volume, the more southerly location of Illinoian moraines raises the possibility of reduced LIS thickness (due to an apparently larger area).

A reduced-volume and thinner LIS could have been more stable and less prone to surging. Hodell et al. (2008) noted that, prior to MIS 4, HS Heinrich Events were limited to the latter portions of each glaciation and attributed this to ice sheet thickness exceeding a threshold that initiated dynamic behavior of the Hudson Strait Ice Stream (e.g., Marshall and Clark, 2002). During MIS 6 (as well as glaciations prior to MIS 16), the conditions needed to induce binge-purge behavior may not have been attained in the Hudson Strait until much later in the glaciation, if at all (Hodell et al., 2008; Naafs et al., 2013).

Regardless of overall thickness and spatial extent of the MIS 6 LIS, other means exist to explain the reduced surging. Steady streaming from a consistently warm-based ice sheet in the Hudson Strait region would produce a relatively constant background level of dolomite. However, the virtual absence of DC and low dolomite content suggest that this was not the case. A cold based ice sheet could also result from cooler summers due to higher orbital eccentricity. This could have reduced basal melting (due to decreased downward heat penetration) and shifted the latitudinal boundary between basal freezing/melting further south, conceivably leaving the Hudson Strait drainage basin under a cold-based ice sheet during the penultimate glacial-equivalent of MIS 3. The results presented here suggest that boundary conditions predispose large Northern Hemisphere ice sheets to millennial fluctuations, and in the absence of an appropriate configuration, large-amplitude glacial variability is driven predominantly by external triggers, becoming primarily orbital in scale.

6. Conclusions

A composite North Atlantic record from DSDP Site 609 and its reoccupation, IODP Site U1308, encompasses the past three glaciations and shows that variability within MIS 6 differs substantially from that exhibited by the two surrounding glaciations. The MIS 8 HSG record exhibits similar cyclicity as the MIS 4–2 record, but the MIS 6 record lacks well-defined cycles, with relatively large-amplitude events spaced at much longer intervals. MIS 8 contains three HS Heinrich Events at ~263, 249, and 243 ka, but there is little evidence for surging in the area of the Hudson Strait during MIS 6, including during the so-called "H11".

During MIS 6, very high background concentrations of lithic grains, primarily derived from sources other than the Hudson Strait region, indicate relatively continuous glacial meltwater input that generally reduced NADW production and increased thermohaline disruption sensitivity. The highest concentration of IRD occurred during high 65°N summer insolation, and relatively weak forcing events, associated with increased material derived from Iceland and perhaps sea ice expansion, ultimately appear to have triggered major MIS 6 climate reorganization during times of low insolation. Apparent ice sheet stability in the Hudson Strait region during MIS 6 may have been partially related to larger variation in eccentricity, leading to cooler summers that shifted the latitudinal boundary between basal freezing/melting farther south, relative to MIS 3, at a time when European ice volume was maximized. Taken together, the results presented here suggest muted D–O variability during MIS 6.

Acknowledgements

This work is dedicated to the late Tom Crowley, whose 40-yr career spanned multiple periods and time scales, from snowball earth, CLIMAP, the last 2000 yr, and most recently, the last 200 (Crowley et al., 2014). Tom was keen to test the idea that the last glaciation is representative of Late Pleistocene glaciations in general, and this work is a contribution to that goal. We thank Rusty Lotti-Bond and Peter Almasi for HSG procedural information, as well as Tokiyuki Sato and Makoto Yamasaki for providing lab space and support. Bruce Corliss, Gary Dwyer, Ayako Abe-Ouchi, Henning Bauch, Axel Timmermann, Peter Abbott, and Azusa Kuroyanagi contributed thoughtful discussion. N. Dobuchi, T. Aze, K. Tsuzuki, M. Greaves, and J. Day provided laboratory assistance. Detailed comments from Ian Bailey and an anonymous reviewer greatly improved this work. We finally thank editor Jean Lynch-Stieglitz. Financial support was provided by JOI/USSSP; JSPS Kakenhi 22101005 and 26247085; the NEXT program GR031; and NERC Grant Number NE/H009930/1. Data included in this manuscript are available at http://dx.doi.org/10.1594/PANGAEA.834640.

Appendix A. Supplementary material

Supplementary material related to this article can be found online at http://dx.doi.org/10.1016/j.epsl.2014.09.004. These data include the Google map of the most important areas described in this article.

References

Abe-Ouchi, A., Saito, F., Kawamura, K., Raymo, M.E., Okuno, J., Takahashi, K., Blatter, H., 2013. Insolation-driven 100,000-year glacial cycles and hysteresis of ice-sheet volume. Nature 500 (7461), 190–193. http://dx.doi.org/10.1038/nature12374.

Ahn, J., Brook, E.J., 2007. Atmospheric CO_2 and climate from 65 to 30 ka B.P. Geophys. Res. Lett. 34 (10). http://dx.doi.org/10.1029/2007GL029551.

Ahn, J., Brook, E.J., 2008. Atmospheric CO_2 and climate on millennial time scales during the last glacial period. Science 322 (5898), 83–85. http://dx.doi.org/10.1126/science.1160832.

Andersen, K.K., Azuma, N., Barnola, J.M., Bigler, M., Biscaye, P., Caillon, N., Chappellaz, J., Clausen, H.B., Dahl-Jensen, D., Fischer, H., Fluckiger, J., Fritzsche, D., Fujii, Y., Goto-Azuma, K., Gronvold, K., Gundestrup, N.S., Hansson, M., Huber, C., Hvidberg, C.S., Johnsen, S.J., Jonsell, U., Jouzel, J., Kipfstuhl, S., Landais, A., Leuenberger, M., Lorrain, R., Masson-Delmotte, V., Miller, H., Motoyama, H., Narita, H., Popp, T., Rasmussen, S.O., Raynaud, D., Rothlisberger, R., Ruth, U., Samyn, D., Schwander, J., Shoji, H., Siggard-Andersen, M.L., Steffensen, J.P., Stocker, T., Sveinbjornsdottir, A.E., Svensson, A., Takata, M., Tison, J.L., Thorsteinsson, T., Watanabe, O., Wilhelms, F., White, J.W.C., 2004. High-resolution record of Northern Hemisphere climate extending into the last interglacial period. Nature 431 (7005), 147–151. http://dx.doi.org/10.1038/nature02805.

Anderson, R.F., Ali, S., Bradtmiller, L.I., Nielsen, S.H.H., Fleisher, M.Q., Anderson, B.E., Burckle, L.H., 2009. Wind-driven upwelling in the Southern Ocean and the deglacial rise in atmospheric CO_2. Science 323 (5920), 1443–1448. http://dx.doi.org/10.1126/science.1167441.

Barker, S., Knorr, G., Edwards, R.L., Parrenin, F., Putnam, A.E., Skinner, L.C., Wolff, E., Ziegler, M., 2011. 800,000 years of abrupt climate variability. Science 334 (6054), 347–351. http://dx.doi.org/10.1126/science.1203580.

Bazin, L., Landais, A., Lemieux-Dudon, B., Toyé Mahamadou Kele, H., Veres, D., Parrenin, F., Martinerie, P., Ritz, C., Capron, E., Lipenkov, V., Loutre, M.-F., Raynaud, D., Vinther, B., Svensson, A., Rasmussen, S.O., Severi, M., Blunier, T., Leuenberger, M., Fischer, H., Masson-Delmotte, V., Chappellaz, J., Wolff, E., 2013. An optimized multi-proxy, multi-site Antarctic ice and gas orbital chronology (AICC2012): 120–800 ka. Clim. Past 9 (4), 1715–1731. http://dx.doi.org/10.5194/cp-9-1715-2013.

Bintanja, R., van de Wal, R.S.W., 2008. North American ice-sheet dynamics and the onset of 100,000-year glacial cycles. Nature 454 (7206), 869–872. http://dx.doi.org/10.1038/nature07158.

Blunier, T., Brook, E.J., 2001. Timing of millennial-scale climate change in Antarctica and Greenland during the last glacial period. Science 291 (5501), 109–112. http://dx.doi.org/10.1126/science.291.5501.109.

Bond, G.C., Lotti, R., 1995. Iceberg discharges into the North-Atlantic on millennial time scales during the last glaciation. Science 267 (5200), 1005–1010. http://dx.doi.org/10.1126/science.267.5200.1005.

Bond, G.C., Heinrich, H., Broecker, W., Labeyrie, L., McManus, J., Andrews, J., Huon, S., Jantschik, R., Clasen, S., Simet, C., Tedesco, K., Klas, M., Bonani, G., Ivy, S., 1992. Evidence for massive discharges of icebergs into the North-Atlantic Ocean during the Last Glacial Period. Nature 360 (6401), 245–249. http://www.nature.com/nature/journal/v360/n6401/abs/360245a0.html.

Bond, G.C., Broecker, W., Johnsen, S., McManus, J., Labeyrie, L., Jouzel, J., Bonani, G., 1993. Correlations between climate records from North-Atlantic sediments and Greenland ice. Nature 365 (6442), 143–147. http://dx.doi.org/10.1038/365143a0.

Bond, G.C., Showers, W., Cheseby, M., Lotti, R., Almasi, P., deMenocal, P., Priore, P., Cullen, H., Hajdas, I., Bonani, G., 1997. A pervasive millennial-scale cycle in North Atlantic Holocene and glacial climates. Science 278 (5341), 1257–1266. http://dx.doi.org/10.1126/science.278.5341.1257.

Bond, G.C., Showers, W., Elliot, M., Evans, M.N., Lotti, R., Hajdas, I., Bonani, G., Johnsen, S., 1999. The North Atlantic's 1–2 kyr climate rhythm: relation to Heinrich events, Dansgaard/Oeschger cycles and the little ice age. In: Clark, P.U., Webb, R.S., Keigwin, L.d. (Eds.), Mechanisms of Global Climate Change at Millennial Time Scales. AGU, Washington DC, pp. 35–58.

Bond, G.C., Kromer, B., Beer, J., Muscheler, R., Evans, M.N., Showers, W., Hoffmann, S., Lotti-Bond, R., Hajdas, I., Bonani, G., 2001. Persistent solar influence on North Atlantic climate during the Holocene. Science 294 (5549), 2130–2136. http://dx.doi.org/10.1126/science.1065680.

Channell, J.E.T., Hodell, D.A., Romero, O., Hillaire-Marcel, C., de Vernal, A., Stoner, J.S., Mazaud, A., Röhl, U., 2012. A 750-kyr detrital-layer stratigraphy for the North Atlantic (IODP Sites U1302–U1303, Orphan Knoll, Labrador Sea). Earth Planet. Sci. Lett. 317–318, 218–230. http://dx.doi.org/10.1016/j.epsl.2011.11.029.

Channell, J.E.T., Hodell, D.A., 2013. Magnetic signatures of Heinrich-like detrital layers in the Quaternary of the North Atlantic. Earth Planet. Sci. Lett. 369–370, 260–270. http://dx.doi.org/10.1016/j.epsl.2013.03.034.

Cheng, H., Edwards, R.L., Broecker, W.S., Denton, G.H., Kong, X., Wang, Y., Zhang, R., Wang, X., 2009. Ice age terminations. Science 326 (5950), 248–252. http://dx.doi.org/10.1126/science.1177840.

Cheng, H., Sinha, A., Cruz, F.W., Wang, X., Edwards, R.L., d'Horta, F.M., Ribas, C.C., Vuille, M., Stott, L.D., Auler, A.S., 2013. Climate change patterns in Amazonia and biodiversity. Nat. Commun. 4. http://dx.doi.org/10.1038/ncomms2415.

Clark, P.U., Mix, A.C., 2002. Ice sheets and sea level of the Last Glacial Maximum. Quat. Sci. Rev. 21 (1–3), 1–7. http://dx.doi.org/10.1016/S0277-3791(01)00118-4.

CLIMAP Project Members, 1976. The surface of the ice-age Earth. Science 19, 1131–1137. http://dx.doi.org/10.1126/science.191.4232.1131.

Crowley, T.J., Hyde, W.T., 2008. Transient nature of late Pleistocene climate variability. Nature 456 (7219), 226–230. http://dx.doi.org/10.1038/nature07365.

Crowley, T.J., 1992. North Atlantic Deep Water cools the Southern hemisphere. Paleoceanography 7 (4), 489–497. http://dx.doi.org/10.1029/92PA01058.

Crowley, T.J., Obrochta, S.P., Liu, J., 2014. Recent global temperature "plateau" in the context of a new proxy reconstruction. Earth's Future 2 (5), 281–294. http://dx.doi.org/10.1002/2013EF000216.

Dansgaard, W., Johnsen, S.J., Clausen, H.B., Dahl-Jensen, D., Gundestrup, N.S., Hammer, C.U., Hvidberg, C.S., Steffensen, J.P., Sveinbjornsdottir, A.E., Jouzel, J., Bond, G., 1993. Evidence for general instability of past climate from a 250-kyr ice-core record. Nature 364 (6434), 218–220. http://dx.doi.org/10.1038/364218a0.

de Abreu, L., Shackleton, N.J., Schönfeld, J., Hall, M., Chapman, M., 2003. Millennial-scale oceanic climate variability off the Western Iberian margin during the last two glacial periods. Mar. Geol. 196 (1–2), 1–20. http://dx.doi.org/10.1016/S0025-3227(03)00046-X.

de Boer, B., Lourens, L.J., van de Wal, R.S.W., 2014. Persistent 400,000-year variability of Antarctic ice volume and the carbon cycle is revealed throughout the Plio-Pleistocene. Nat. Commun. 5. http://dx.doi.org/10.1038/ncomms3999.

Denton, G.H., Anderson, R.F., Toggweiler, J.R., Edwards, R.L., Schaefer, J.M., Putnam, A.E., 2010. The last glacial termination. Science 328 (5986), 1652–1656. http://dx.doi.org/10.1126/science.1184119.

Didié, C., Bauch, H.A., 2000. Species composition and glacial–interglacial variations in the ostracode fauna of the northeast Atlantic during the past 200,000 years. Mar. Micropaleontol. 40 (1–2), 105–129. http://dx.doi.org/10.1016/S0377-8398(00)00034-7.

Ditlevsen, P.D., Andersen, K.K., Svensson, A., 2007. The DO-climate events are probably noise induced: statistical investigation of the claimed 1470 years cycle. Clim. Past 3 (1), 129–134. http://dx.doi.org/10.5194/cp-3-129-2007.

Downing, G., 2008. Variability of North Atlantic ice rafting during the last two glaciations. PhD thesis. Columbia University.

Ehlers, J., Grube, A., Stephan, H.-J., Wansa, S., 2011. Pleistocene glaciations of North Germany—new results. In: Ehlers, J., Gibbard, P.L., Hughes, P.D. (Eds.), Quaternary Glaciations – Extent and Chronology a Closer Look. Elsevier, pp. 149–162.

Elliot, M., Labeyrie, L., Bond, G.C., Cortijo, E., Turon, J.-L., Tisnerat, N., Duplessy, J.-C., 1998. Millennial-scale iceberg discharges in the Irminger Basin during the last glacial period: relationship with the Heinrich events and environmental settings. Paleoceanography 13 (5), 433–446. http://dx.doi.org/10.1029/98PA01792.

EPICA Community Members, 2006. One-to-one coupling of glacial climate variability in Greenland and Antarctica. Nature 444 (7116), 195–198. http://dx.doi.org/10.1038/nature05301.

Expedition 303 Scientists, 2006. Site U1308. In: Proceedings of the Integrated Ocean Drilling Program, vol. 303/306.

Forman, S.L., Pierson, J., 2002. Late Pleistocene luminescence chronology of loess deposition in the Missouri and Mississippi river valleys, United States. Palaeogeogr. Palaeoclimatol. Palaeoecol. 186 (1–2), 25–46. http://dx.doi.org/10.1016/S0031-0182(02)00440-6.

Ghil, M., Allen, M.R., Dettinger, M.D., Ide, K., Kondrashov, D., Mann, M.E., Robertson, A.W., Saunders, A., Tian, Y., Varadi, F., Yiou, P., 2002. Advanced spectral methods for climatic time series. Rev. Geophys. 40 (1). http://dx.doi.org/10.1029/2000RG000092.

Greaves, M., Barker, S., Daunt, C., Elderfield, H., 2005. Accuracy, standardisation and interlaboratory calibration standards for foraminiferal Mg/Ca thermometry. Geochem. Geophys. Geosyst. 6, Q02D13. http://dx.doi.org/10.1029/2004GC000790.

Hall, I.R., McCave, I.N., 2000. Palaeocurrent reconstruction, sediment and thorium focussing on the Iberian margin over the last 140 ka. Earth Planet. Sci. Lett. 178 (1–2), 151–164. http://dx.doi.org/10.1016/S0012-821X(00)00068-6.

Heinrich, H., 1988. Origin and consequences of cyclic ice rafting in the Northeast Atlantic Ocean during the past 130,000 years. Quat. Res. 29 (2), 142–152. http://dx.doi.org/10.1016/0033-5894(88)90057-9.

Hemming, S.R., 2004. Heinrich events: massive late Pleistocene detritus layers of the North Atlantic and their global climate imprint. Rev. Geophys. 42 (1). http://dx.doi.org/10.1029/2003RG000128.

Hillaire-Marcel, C., de Vernal, Anne, 2008. Stable isotope clue to episodic sea ice formation in the glacial North Atlantic. Earth Planet. Sci. Lett. 268 (1–2), 143–150. http://dx.doi.org/10.1016/j.epsl.2008.01.012.

Hodell, D.A., Curtis, J.H., 2008. Oxygen and carbon isotopes of detrital carbonate in North Atlantic Heinrich Events. Mar. Geol. 256 (1–4), 30–35. http://dx.doi.org/10.1016/j.margeo.2008.09.010.

Hodell, D.A., Channell, J.E.T., Curtis, J.H., Romero, O.E., Röhl, U., 2008. Onset of "Hudson Strait" Heinrich events in the eastern North Atlantic at the end of the middle Pleistocene transition (~640 ka)? Paleoceanography 23. http://dx.doi.org/10.1029/2008PA001591.

Ji, J., Ge, Y., Balsam, W., Damuth, J.E., Chen, J., 2009. Rapid identification of dolomite using a Fourier Transform Infrared Spectrophotometer (FTIR): a fast method for identifying Heinrich events in IODP Site U1308. Mar. Geol. 258 (1–4), 60–68. http://dx.doi.org/10.1016/j.margeo.2008.11.007.

Jouzel, J., Masson-Delmotte, V., Cattani, O., Dreyfus, G., Falourd, S., Hoffmann, G., Minster, B., Nouet, J., Barnola, J.M., Chappellaz, J., Fischer, H., Gallet, J.C., Johnsen, S., Leuenberger, M., Loulergue, L., Luethi, D., Oerter, H., Parrenin, F., Raisbeck, G., Raynaud, D., Schilt, A., Schwander, J., Selmo, E., Souchez, R., Spahni, R., Stauffer, B., Steffensen, J.P., Stenni, B., Stocker, T.F., Tison, J.L., Werner, M., Wolff, E.W., 2007. Orbital and millennial Antarctic climate variability over the past 800,000 years. Science 317 (5839), 793–796. http://dx.doi.org/10.1126/science.1141038.

Kanner, L.C., Burns, S.J., Cheng, H., Edwards, R.L., 2012. High-latitude forcing of the South American Summer Monsoon during the last glacial. Science 335 (6068), 570–573. http://dx.doi.org/10.1126/science.1213397.

Kubota, K., Yokoyama, Y., Ishikawa, T., Obrochta, S., Suzuki, A., 2014. Larger CO_2 source at the equatorial Pacific during the last deglaciation. Sci. Rep. 4. http://dx.doi.org/10.1038/srep05261.

Kuhs, M., Austin, W.E.N., Abbott, P.M., Hodell, D.A., 2014. Iceberg-rafted Tephra as a potential tool for the reconstruction of ice-sheet processes and ocean surface circulation in the Glacial North Atlantic. Geol. Soc. (Lond.) Spec. Publ., 398. http://dx.doi.org/10.1144/SP398.8.

Lambeck, K., Purcell, A., Funder, S., Kjær, K., Larsen, E., Möller, P., 2006. Constraints on the Late Saalian to early Middle Weichselian ice sheet of Eurasia from field data and rebound modelling. Boreas 35 (3), 539–575. http://dx.doi.org/10.1080/03009480600781875.

Li, T.-Y., Shen, C.-C., Huang, L.-J., Jiang, X.-Y., Yang, X.-L., Mii, H.-S., Lee, S.-Y., Lo, L., 2014. Stalagmite-inferred variability of the Asian summer monsoon during the penultimate glacial–interglacial period. Clim. Past 10 (3), 1211–1219. http://www.clim-past.net/10/1211/2014/.

Lisiecki, L.E., Raymo, M.E., 2005. A Pliocene–Pleistocene stack of 57 globally distributed benthic O-18 records. Paleoceanography 20. http://dx.doi.org/10.1029/2004PA001071.

Manabe, S., Broccoli, A.J., 1985. The influence of continental ice sheets on the climate of an ice age. J. Geophys. Res. 90, 2167–2190.

Manabe, S., Stouffer, R.J., 1988. Two stable equilibria of a coupled ocean-atmosphere model. J. Climate 1 (9), 844–866. http://dx.doi.org/10.1175/1520-0442(1988)001<0841:TSEOAC>2.0.CO;2.

Margari, V., Skinner, L.C., Tzedakis, P.C., Ganopolski, A., Vautravers, M., Shackleton, N.J., 2010. The nature of millennial-scale climate variability during the past two glacial periods. Nat. Geosci. 3 (2), 127–131. http://dx.doi.org/10.1038/ngeo740.

Margari, V., Skinner, L.C., Hodell, D.A., Martrat, B., Toucanne, S., Grimalt, J.O., Gibbard, P.L., Lunkka, J.P., Tzedakis, P.C., 2014. Land–ocean changes on orbital and millennial time scales and the penultimate glaciation. Geology 42 (3), 183–186. http://dx.doi.org/10.1130/G35070.1.

Marshall, S.J., Clark, P.U., 2002. Basal temperature evolution of North American ice sheets and implications for the 100-kyr cycle. Geophys. Res. Lett. 29. http://dx.doi.org/10.1029/2002GL015192.

Marshall, S.J., Koutnik, M.R., 2006. Ice sheet action versus reaction: distinguishing between Heinrich events and Dansgaard–Oeschger cycles in the North Atlantic. Paleoceanography 21. http://dx.doi.org/10.1029/2005PA001247.

Martrat, B., Grimalt, J.O., Shackleton, N.J., de Abreu, L., Hutterli, M.A., Stocker, T.F., 2007. Four climate cycles of recurring deep and surface water destabilizations on the Iberian Margin. Science 317 (5837), 502–507. http://dx.doi.org/10.1126/science.1139994.

McCave, I.N., Manighetti, B., Beveridge, N.A.S., 1995. Circulation in the glacial North-Atlantic inferred from grain-size measurements. Nature 374 (6518), 149–152. http://dx.doi.org/10.1038/374149a0.

McManus, J.F., Oppo, D.W., Cullen, J.L., 1999. A 0.5-million-year record of millennial-scale climate variability in the North Atlantic. Science 283 (5404), 971–975. http://dx.doi.org/10.1126/science.283.5404.971.

Menviel, L., Timmermann, A., Friedrich, T., England, M.H., 2014. Hindcasting the continuum of Dansgaard–Oeschger variability: mechanisms, patterns and timing. Clim. Past 10 (1), 63–77. http://dx.doi.org/10.5194/cp-10-63-2014.

Mohtadi, M., Oppo, D.W., Steinke, S., Stuut, J.-B.W., De P.-H., Ricardo, Hebbeln, D., Luckge, A., 2011. Glacial to Holocene swings of the Australian–Indonesian monsoon. Nat. Geosci. 4 (8), 540–544. http://dx.doi.org/10.1038/ngeo1209.

Muller, J., Kylander, M., Wüst, R.A.J., Weiss, D., Martinez-Cortizas, A., LeGrande, A.N., Jennerjahn, T., Behling, H., Anderson, W.T., Jacobson, G., 2008. Possible evidence for wet Heinrich phases in tropical NE Australia: the Lynch's Crater deposit. Quat. Sci. Rev. 27 (5–6), 468–475. http://dx.doi.org/10.1016/j.quascirev.2007.11.006.

Naafs, B.D.A., Hefter, J., Ferretti, P., Stein, R., Haug, G.H., 2011. Sea surface temperatures did not control the first occurrence of Hudson Strait Heinrich events during MIS 16. Paleoceanography 26 (4), PA4201. http://dx.doi.org/10.1029/2011PA002135.

Naafs, B.D.A., Hefter, J., Stein, R., 2013. Millennial-scale ice rafting events and Hudson Strait Heinrich(-like) events during the late Pliocene and Pleistocene: a review. Quat. Sci. Rev. 80, 1–28. http://dx.doi.org/10.1016/j.quascirev.2013.08.014.

Nace, T.E., Dwyer, G.S., Silva, C.G., Rigsby, C.A., Burns, S.J., Giosan, L., Otto-Bliesner, B., Liu, Z., Zhu, J., Hollander, D., Baker, P.A., 2014. The role of North Brazil Current transport in the paleoclimate of the Brazilian Nordeste margin and paleoceanography of the western tropical Atlantic during the late Quaternary. Palaeogeogr. Palaeoclimatol. Palaeoecol.. http://dx.doi.org/10.1016/j.palaeo.2014.05.030.

Obrochta, S.P., Miyahara, H., Yokoyama, Y., Crowley, T.J., 2012. A re-examination of evidence for the North Atlantic "1500-year cycle" at Site 609. Quat. Sci. Rev. 55, 23–33. http://dx.doi.org/10.1016/j.quascirev.2012.08.008.

Obrochta, S.P., Yokoyama, Y., Morén, J., Crowley, T.J., 2014. Conversion of GISP2-based sediment core age models to the GICC05 extended chronology. Quat. Geochronol. 20, 1–7. http://dx.doi.org/10.1016/j.quageo.2013.09.001.

Oka, A., Hasumi, H., Abe-Ouchi, A., 2012. The thermal threshold of the Atlantic meridional overturning circulation and its control by wind stress forcing during glacial climate. Geophys. Res. Lett. 39 (9), L09709. http://dx.doi.org/10.1029/2012GL051421.

Oppo, D.W., McManus, J.F., Cullen, J.L., 2006. Evolution and demise of the last interglacial warmth in the subpolar North Atlantic. Quat. Sci. Rev. 25 (23–24), 3268–3277. http://dx.doi.org/10.1016/j.quascirev.2006.07.006.

Ortiz, J., Mix, A., Harris, S., O'Connell, S., 1999. Diffuse spectral reflectance as a proxy for percent carbonate content in North Atlantic sediments. Paleoceanography 14 (2), 171–186. http://dx.doi.org/10.1029/1998PA900021.

Rasmussen, S.O., Andersen, K.K., Svensson, A.M., Steffensen, J.P., Vinther, B.M., Clausen, H.B., Siggaard-Andersen, M.-L., Johnsen, S.J., Larsen, L.B., Dahl-Jensen, D., Bigler, M., Röthlisberger, R., Fischer, H., Goto-Azuma, K., Hansson, M.E., Ruth, U., 2006. A new Greenland ice core chronology for the last glacial termination. J. Geophys. Res., Atmos. 111 (D6). http://dx.doi.org/10.1029/2005JD006079.

Reimer, P.J., Baillie, M.G.L., Bard, E., Bayliss, A., Beck, J.W., Blackwell, P.G., BronkRamsey, C., Buck, C.E., Burr, G.S., Edwards, R.L., Friedrich, M., Grootes, P.M., Guilderson, T.P., Hajdas, I., Heaton, T.J., Hogg, A.G., Hughen, K.A., Kaiser, K.F., Kromer, B., McCormac, F.G., Manning, S.W., Reimer, R.W., Richards, D.A., Southon, J.R., Talamo, S., Turney, C.S.M., vanderPlicht, J., Weyhenmeyer, C.E., 2009. IntCal09 and Marine09 radiocarbon age calibration curves, 0–50,000 years cal BP. Radiocarbon 51 (4), 1111–1150. https://journals.uair.arizona.edu/index.php/radiocarbon/article/view/3569/3082.

Ruddiman, W.F., 1977. Late Quaternary deposition of ice-rafted sand in the subpolar North Atlantic (lat 40 degrees to 65 degrees N). Geol. Soc. Am. Bull. 88 (12), 1813–1827. http://dx.doi.org/10.1130/0016-7606(1977)88<1813:LQDOIS>2.0.CO;2.

Ruddiman, W.F., Kidd, R.B., Thomas, E., Shipboard Scientific Party, 1987. Initial reports of the Deep Sea Drilling Project. 94. http://www.deepseadrilling.org/94/dsdp_toc.htm.

Shackleton, N.J., Hall, M.A., Vincent, E., 2000. Phase relationships between millennial-scale events 64,000–24,000 years ago. Paleoceanography 15 (6), 565–569. http://dx.doi.org/10.1029/2000PA000513.

Stein, R., Hefter, J., Grützner, J., Voelker, A., Naafs, B.D.A., 2009. Variability of surface water characteristics and Heinrich-like events in the Pleistocene midlatitude North Atlantic Ocean: biomarker and XRD records from IODP Site U1313 (MIS 16–9). Paleoceanography 19 (2), 149–162. http://dx.doi.org/10.1029/2008PA001639.

Svendsen, J.I., Alexanderson, H., Astakhov, V.I., Demidov, I., Dowdeswell, J.A., Funder, S., Gataullin, V., Henriksen, M., Hjort, C., Houmark-Nielsen, M., Hubberten, H.W., 2004. Ingólfsson, Ó, Jakobsson, M., Kjær, K.H., Larsen, E., Lokrantz, H., Lunkka, J.P., Lyså, A., Mangerud, J., Matiouchkov, A., Murray, A., Möller, P., Niessen, F., Nikolskaya, O., Polyak, L., Saarnisto, M., Siegert, C., Siegert, M.J., Spielhagen, R.F., Stein, R., Late Quaternary ice sheet history of northern Eurasia. Quat. Sci. Rev. 23 (11–13), 1229–1271. http://dx.doi.org/10.1016/j.quascirev.2003.12.008.

Svensson, A., Andersen, K.K., Bigler, M., Clausen, H.B., Dahl-Jensen, D., Davies, S.M., Johnsen, S.J., Muscheler, R., Parrenin, F., Rasmussen, S.O., Röthlisberger, R., Seierstad, I., Steffensen, J.P., Vinther, B.M., 2008. A 60 000 year Greenland stratigraphic ice core chronology. Clim. Past 4 (1), 47–57. http://dx.doi.org/10.5194/cp-4-47-2008.

Timmermann, A., Knies, J., Timm, O.E., Abe-Ouchi, A., Friedrich, T., 2010. Promotion of glacial ice sheet buildup 60–115 kyr B.P. by precessionally paced Northern Hemispheric meltwater pulses. Paleoceanography 25 (4), PA4208. http://dx.doi.org/10.1029/2010PA001933.

Toucanne, S., Zaragosi, S., Bourillet, J.F., Cremer, M., Eynaud, F., Van Vliet-Lanoë, B., Penaud, A., Fontanier, C., Turon, J.L., Cortijo, E., Gibbard, P.L., 2009. Timing of massive 'Fleuve Manche' discharges over the last 350 kyr: insights into the European ice-sheet oscillations and the European drainage network from MIS 10 to 2. Quat. Sci. Rev. 28 (13–14), 1238–1256. http://dx.doi.org/10.1016/j.quascirev.2009.01.006.

Veres, D., Bazin, L., Landais, A., Toyé Mahamadou Kele, H., Lemieux-Dudon, B., Parrenin, F., Martinerie, P., Blayo, E., Blunier, T., Capron, E., Chappellaz, J., Rasmussen, S.O., Severi, M., Svensson, A., Vinther, B., Wolff, E.W., 2013. The Antarctic ice core chronology (AICC2012): an optimized multi-parameter and multi-site dating approach for the last 120 thousand years. Clim. Past 9 (4), 1733–1748. http://dx.doi.org/10.5194/cp-9-1733-2013.

Wang, Y.J., Cheng, H., Edwards, R.L., An, Z.S., Wu, J.Y., Shen, C.-C., Dorale, J.A., 2001. A high-resolution absolute-dated late Pleistocene Monsoon record from Hulu Cave, China. Science 294 (5550), 2345–2348. http://dx.doi.org/10.1126/science.1064618.

Wang, X., Auler, A.S., Edwards, R.L., Cheng, H., Cristalli, P.S., Smart, P.L., Richards, D.A., Shen, C.-C., 2004. Wet periods in northeastern Brazil over the past 210-kyr linked to distant climate anomalies. Nature 432 (7018), 740–743. http://dx.doi.org/10.1038/nature03067.

Wang, Y., Cheng, H., Edwards, R.L., Kong, X., Shao, X., Chen, S., Wu, J., Jiang, X., Wang, X., An, Z., 2008. Millennial- and orbital-scale changes in the East Asian monsoon over the past 224,000 years. Nature 451 (7182), 1090–1093. http://dx.doi.org/10.1038/nature06692.

Weldeab, S., Lea, D.W., Schneider, R.R., Andersen, N., 2007. 155,000 years of West African monsoon and ocean thermal evolution. Science 316 (5829), 1303–1307. http://dx.doi.org/10.1126/science.1140461.

Wolff, E.W., Chappellaz, J., Blunier, T., Rasmussen, S.O., Svensson, A., 2010. Millennial-scale variability during the last glacial: the ice core record. Quat. Sci. Rev. 29 (21–22), 2828–2838. http://dx.doi.org/10.1016/j.quascirev.2009.10.013.

Yokoyama, Y., Esat, T.M., 2011. Global climate and sea level: enduring variability and rapid fluctuations over the past 150,000 years. Oceanography 24 (2), 54–69. http://dx.doi.org/10.5670/oceanog.2011.27.

Yokoyama, Y., Esat, T.M., Lambeck, K., 2001a. Coupled climate and sea-level changes deduced from Huon Peninsula coral terraces of the last ice age. Earth Planet. Sci. Lett. 193 (3–4), 579–587. http://dx.doi.org/10.1016/S0012-821X(01)00515-5.

Yokoyama, Y., Esat, T.M., Lambeck, K., 2001b. Last glacial sea-level change deduced from uplifted coral terraces of Huon Peninsula, Papua New Guinea. Quat. Int. 83 (35), 275–278. http://dx.doi.org/10.1016/S1040-6182(01)00045-3.